

9-1-2016

Expanding the Applicability of Raman Spectroscopy for Monitoring Photocatalytic Degradation

Franklyn Wallace

Western Kentucky University, frankie.wallace664@topper.wku.edu

Follow this and additional works at: http://digitalcommons.wku.edu/stu_hon_theses

 Part of the [Environmental Chemistry Commons](#), and the [Environmental Indicators and Impact Assessment Commons](#)

Recommended Citation

Wallace, Franklyn, "Expanding the Applicability of Raman Spectroscopy for Monitoring Photocatalytic Degradation" (2016). *Honors College Capstone Experience/Thesis Projects*. Paper 668.
http://digitalcommons.wku.edu/stu_hon_theses/668

This Thesis is brought to you for free and open access by TopSCHOLAR®. It has been accepted for inclusion in Honors College Capstone Experience/Thesis Projects by an authorized administrator of TopSCHOLAR®. For more information, please contact topscholar@wku.edu.

EXPANDING THE APPLICABILITY OF RAMAN SPECTROSCOPY FOR
MONITORING PHOTOCATALYTIC DEGRADATION

A Capstone Experience/Thesis Project

Presented in Partial Fulfillment of the Requirements for

the Degree Bachelor of Science with

Honors College Graduate Distinction at Western Kentucky University

By

Franklyn K. Wallace

Western Kentucky University
2016

CE/T Committee:

Dr. Matthew Nee, Advisor

Dr. Darwin Dahl

Dr. Lester Pesterfield

Approved By

Advisor
Department of Chemistry

Copyright by
Franklyn K. Wallace
2016

ABSTRACT

Compared to other types of wastewater pollutants, dangerous chemical compounds such as pharmaceuticals, pesticides, and herbicides are difficult to remove and consequently being detected (at least in part because detection limits have decreased) in drinking water at increasing concentrations. Photocatalytic degradation degrades harmful compounds to innocuous end products using energy from light. Although it is effective and cost-efficient, the underlying chemical mechanisms are not understood well enough to ensure that dangerous intermediate products are not formed during the degradation process. Raman spectroscopy can be used to analyze photocatalytic degradation reactions in real time, identifying intermediate products based on spectral features. Due to fast data acquisition, Raman studies can identify those intermediate products which are short-lived and could be missed by slower conventional methods. In the current research, colloidal gold nanoparticles were introduced to increase sensitivity via surface-enhanced Raman spectroscopy (SERS), and later modified to maintain signal intensity over a longer period of time. Additionally, an internal standard was introduced for ratiometric determination of analyte concentration. These procedural modifications serve to expand the applicability of Raman spectroscopy for *in-situ* reaction monitoring.

Keywords: environmental chemistry, water treatment, herbicides, SERS, photocatalytic degradation, nanoparticles

Dedicated to my dog, Annie

ACKNOWLEDGEMENTS

I would first like to acknowledge my research mentor, Dr. Matthew Nee, who has had tremendous patience with me as I have grown as a scientist, invested countless hours helping me improve my scientific writing and communication skills, always takes the time to explain concepts which I do not initially understand, and demonstrates greater commitment to professional development of his lab members and students than anyone I know. I would also like to recognize the other members of my thesis defense committee, Dr. Darwin Dahl and Dr. Lester Pesterfield, for their time commitment and willingness to accept the responsibility of reviewing my defense. I am thankful to my parents for always allowing me to pursue my interests, demonstrating proper morals, encouraging my successes, and loving me unconditionally. I would also like to thank my grandparents, not only for their interest and support for me in all aspects of my life, but for allowing me to stay with them during the summer I worked on this project. I could not begin to adequately acknowledge all of the people who have supported and encouraged me as I have worked on this project, so to all of my coworkers, family, and friends; thank you.

Funding for this project was provided by the Kentucky Wastewater Resources Research institute (KWRRRI), WKU faculty-undergraduate student engagement (FUSE), and WKU CE/T excellence grant programs.

VITA

December 27, 1994.....	Born-Georgetown Kentucky
2013.....	Scott County High School, Georgetown, Kentucky
2013.....	WKU Regents Tuition Scholarship
2014.....	Dr. James H. Stuteville Scholarship
2014.....	Georgetown POW/MIA Scholarship
2014.....	Chemistry Club: Secretary
2014.....	Alpha Epsilon Delta: Active Member
2015.....	Chemistry Club: President
2015.....	University of Kentucky Professional Education Preparation Program
2015.....	Chemistry/Biology Tutor; Gatton Academy of Mathematics and Science
2016.....	Teaching Assistant; WKU Department of Physics
2016.....	Christian Health Center, Bowling Green, KY; State Registered Nursing Assistant

2016.....Barry M. Goldwater Honorable
Mention

PRESENTATIONS

- 1) Western Kentucky University 46th Annual Student Research Conference. Bowling Green, KY. “Use of surface enhanced Raman spectroscopy to monitor photocatalytic reactions” F. Wallace and M. J. Nee (April 2016)
- 2) Posters-at-the-Capitol 15th Annual Meeting. Frankfort, KY. “Analytically assessing the safety of innovative technologies in the future of wastewater treatment” F. Wallace and M. J. Nee (February 2016)
- 3) Kentucky Academy of Science 101st Annual Meeting. Highland Heights, KY. “Raman spectroscopy as an analytical tool for monitoring photocatalytic degradation” F. Wallace and M. J. Nee (November, 2015)
- 4) American Chemical Society 250th National Meeting and Exposition. Boston, MA. “Surface enhanced Raman spectroscopy to study photocatalytic degradation of organic pollutants” F. Wallace and M. J. Nee (August, 2015)
- 5) Western Kentucky University Student Research Conference. Bowling Green, KY. “Surface enhanced Raman spectroscopy to study photocatalytic degradation of organic pollutants” F. Wallace and M. J. Nee. (March, 2015) -1st Place Undergraduate Natural Sciences Oral Section
- 6) Kentucky Water Resources Annual Symposium. Lexington, KY. “Surface enhanced Raman spectroscopy to study photocatalytic degradation of organic pollutants” F. Wallace and M. J. Nee. (March, 2015)
- 7) Kentucky Academy of Science 100th Annual Meeting. Lexington, KY. “Use of carbon disulfide as an internal standard for SERS experiments.” F. Wallace and M. J. Nee (November, 2014) -2nd Place Undergraduate Physical/Analytical Chemistry Poster Session
- 8) South Eastern Regional Meeting of the American Chemical Society. Nashville, TN. “Use of carbon disulfide as an internal standard for SERS experiments.” F. Wallace and M. J. Nee (October, 2014)

FIELDS OF STUDY

Major Field 1: Biochemistry

Major Field 2: Chemistry (General)

Minor Field 1: Biophysics

Minor Field 2: Neuroscience

TABLE OF CONTENTS

	<u>Page</u>
Abstract.....	ii
Dedication.....	iii
Acknowledgements.....	iv
Vita.....	v
List of Charts/Schemes.....	x
List of Figures.....	xi
 Chapters:	
1. Introduction: Safe Elimination of Dangerous Wastewater Pollutants.....	1
1.1 Wastewater Treatment.....	1
1.2 Photocatalytic Degradation.....	4
1.3 Chromatographic Procedures (Traditional Analysis).....	7
1.4 Absorption Spectrophotometry/Spectroscopy.....	10
1.5 Project Goals: Expanding applicability.....	12
1.6 Compounds of Interest.....	13
2. Experimental Methods: Tools for Monitoring Photocatalytic Degradation.....	17
2.1 Raman Scattering.....	17
2.2 Raman Spectroscopy.....	19
2.3 Surface-Enhanced Raman Spectroscopy.....	23

	<u>Page</u>
2.4 Nanoparticle Synthesis.....	24
2.5 Nanoparticle Characterization.....	26
2.6 Colloidal Aggregation.....	30
2.7 Secondary Capping.....	31
2.8 Calibration Curve Generation.....	35
2.9 Reaction Monitoring Setup.....	37
3. Results/Discussion: Addressing the Limitations of Raman Spectroscopy.....	40
3.1 UV/VIS and TEM of Nanoparticles.....	41
3.2 Increasing Sensitivity via Surface-Enhanced Raman Spectroscopy.....	43
3.3 Calibration Curves for Quantitative Purposes.....	50
3.4 Initial Reaction Monitoring.....	54
3.5 Nanoparticle Stability.....	56
3.6 Calibration Curves with Secondarily-Capped Nanoparticles.....	63
4. Summary/Future Directions: Effective Reaction Monitoring	68
References.....	73

LIST OF SCHEMES/CHARTS

	<u>Page</u>
Scheme:	
1.1: Methylene blue phototcatalytic degradation scheme.....	9
Chart:	
1.1: Structures for compounds of interest.....	14

LIST OF FIGURES

<u>Figure</u>	<u>Page</u>
1.1 Photocatalytic degradation general mechanism.....	5
2.1 Scattering: Jablonski energy level diagram.....	18
2.2 Block diagram of Raman system.....	20
2.3 Raman nitrate ion example.....	22
2.4 Nanoparticle synthesis.....	25
2.5 Particle in a box.....	28
2.6 Nanoparticle stabilization via decanethiol.....	34
2.7 Reaction monitoring setup.....	38
3.1 Image of colloidal gold nanoparticles.....	41
3.2 Nanoparticle characterization.....	42
3.3 Raman spectrum of colloid alone.....	44
3.4 R6G SERS.....	46
3.5 Computational and SERS paraquat data.....	48
3.6 Paraquat stretch.....	49
3.7 R6G coupled to internal standard.....	51
3.8 Paraquat coupled to internal standard.....	52
3.9 Ratiometric approach R6G.....	53

	<u>Page</u>
3.10 Preliminary R6G calibration curves.....	55
3.11 Photocatalytic degradation initial control trial.....	57
3.12 Aggregation demonstration using nitrate.....	59
3.13 UV/VIS aggregated/un-aggregated comparison.....	62
3.14 Nanoparticle stability demonstration.....	64
3.15 New calibration curve.....	65

CHAPTER 1

Introduction: Safe Elimination of Dangerous Wastewater Pollutants

1.1 Wastewater Treatment

Due to its direct relevance to health, ecological preservation, and environmental protection, maintaining a high level of water quality is a growing concern. The need for adequate wastewater treatment is often discussed as one of the international crises of our era.¹ The wastewater treatment process must effectively eliminate several different types of contaminants in order to ensure adequate water purity.^{2,3} Among the most important categories of contaminants to consider in the wastewater treatment process are large-scale, metal, biological, and chemical contaminants.

The first three types of contaminants are relatively well-regulated in most developed countries. Large-scale contaminants refer to any substance in a waste stream which is insoluble, and thus can be removed. Examples of this type of contaminant include soil, sand, rock, feces, garbage, etc. This is the simplest type of contaminant to remove from wastewater, as it can be done through simple filtration; a physical process which relies on size. Another type of pollutant in wastewater is heavy metals, which can induce severe physiological symptoms and developmental abnormalities to organisms exposed to them. The dangers of heavy metals in wastewater has drawn considerable public attention recently as a result of the emergency situation in Flint, Michigan due to lead contamination

in public drinking water. Many heavy metal elimination procedures focus on the interaction between the metals in water and some stationary substrate. Heavy metals are present as positively charged ions in water, and thus can be removed to some degree by passing them through a filtration channel filled with beads containing negatively charged functional groups.⁴ The interaction between positively charged metal ions in the wastewater and the immobile beads in the filtration channel causes the metal ions to remain in the channel, with the purified water passing through. Although this method is effective in small-scale water purification such as retail personal water filters, it is difficult and expensive to employ on a larger scale. As a result, more recent efforts have dealt primarily with biotechnology, inducing immobilized algae or plants to uptake harmful metal ions from wastewater.^{5,6} The major concern with this method is the potential for biological by-product formation, which can be somewhat controlled by making additional modifications to the algal or plant strains. The use of living organisms for the purpose of wastewater treatment should not be confused with biological contaminants, which are pathogenic species of microorganisms present in wastewater. These species can be removed in many ways, but their treatment is most commonly quite similar to the other discussed contaminants. Ultrafiltration processes can remove some bacteria, and their tendency to physically adsorb onto available substrates is also exploited, analogous to that seen in metals.⁷ One wastewater treatment process that is unique to the removal of biological contaminants is treatment of the wastewater with harsh environments in which most living organisms cannot survive. This includes high temperature and pressure, limiting access to oxygen and nitrogen sources, exposure to harsh chemicals such as chlorine, and radiation treatment.⁸

Although removal of large-scale, metal, and biological contaminants is relatively straight-forward, removal of chemical pollutants is more difficult, causing a continued increase in the concentrations of harmful organic compounds such as pharmaceuticals, pesticides, and herbicides in drinking water.⁹ Chemical pollutants are often colorless, and can have harmful effects even at concentrations which are difficult to detect. These concentrations are also below those which can feasibly be removed via filtration or extraction techniques. Although some compounds can be eliminated from wastewater via processes analogous to those discussed for metals, in which the pollutant is removed based on its affinity for a particular substrate, this is not an easily scalable method since it requires different columns for an enormous variety of compound classes in order to ensure adequate removal.¹⁰ This approach is not only practically difficult to implement, but it would also be economically unfavorable, as the cost associated with its development and upkeep would be high. Some chemical pollutants can also be removed via biotechnology, in which biological organisms break down compounds into innocuous end products, however this is expensive, difficult to scale and control, and can lead to the formation of uncontrolled biological by-products.¹¹ Other common wastewater treatment methods investigated for the removal of wastewater pollutants include chemical methods such as chlorination¹² and ozonation,¹³ which are effective for particular subsets of pollutants, but are known to generate harmful by-products like trihalomethanes and unsaturated hydrocarbons. It is therefore evident that the removal of chemical pollutants from wastewater is not as well-developed as the removal of other pollutant categories. For this reason, some recent efforts related to wastewater treatment have been focused on developing safe, reliable, economical, and broadly applicable methods for eliminating chemical pollutants.

1.2 Photocatalytic Degradation

Some of the most popular technologies proposed for the removal of harmful chemical pollutants from wastewater take advantage of an advanced oxidative process known as photocatalytic degradation.¹⁴ Generally speaking, photocatalytic degradation uses energy from ultra-violet (UV) radiation to ultimately degrade large organic compounds to innocuous end products such as carbon dioxide and water.¹⁵ Photocatalytic degradation is able to eliminate harmful organic compounds relatively quickly, generating less harmful end products such as carbon dioxide and water. Practical implementation is economical since UV radiation from the sun is sufficient to yield significant degradation of some compounds in under three hours, and the photocatalyst which is most commonly used for these purposes is the anatase form of titanium dioxide, a naturally occurring mineral crystal which is inexpensive relative to other potential options.¹⁴ Although a considerable amount of work has focused on increasing reaction efficiency or decreasing costs, too little is known about the mechanism by which photocatalytic degradation acts to ensure its safety in the wastewater treatment process.

Photocatalytic degradation is often classified by one of two general mechanisms depicted in Figure 1.1: degradation via successive hydroxyl radical attack, and direct oxidation via electron holes. Here, an “electron hole” simply refers to the lack of an electron in a region where it would normally be expected to exist. Since oxidation by electron holes requires direct adsorption of the analyte onto TiO_2 , it has varying impacts on the photocatalytic degradation of separate pollutants, and those which do not adsorb onto TiO_2 are not affected by this mechanism. For this reason, these general mechanisms are often discussed as if they are independent of one another. However, when direct

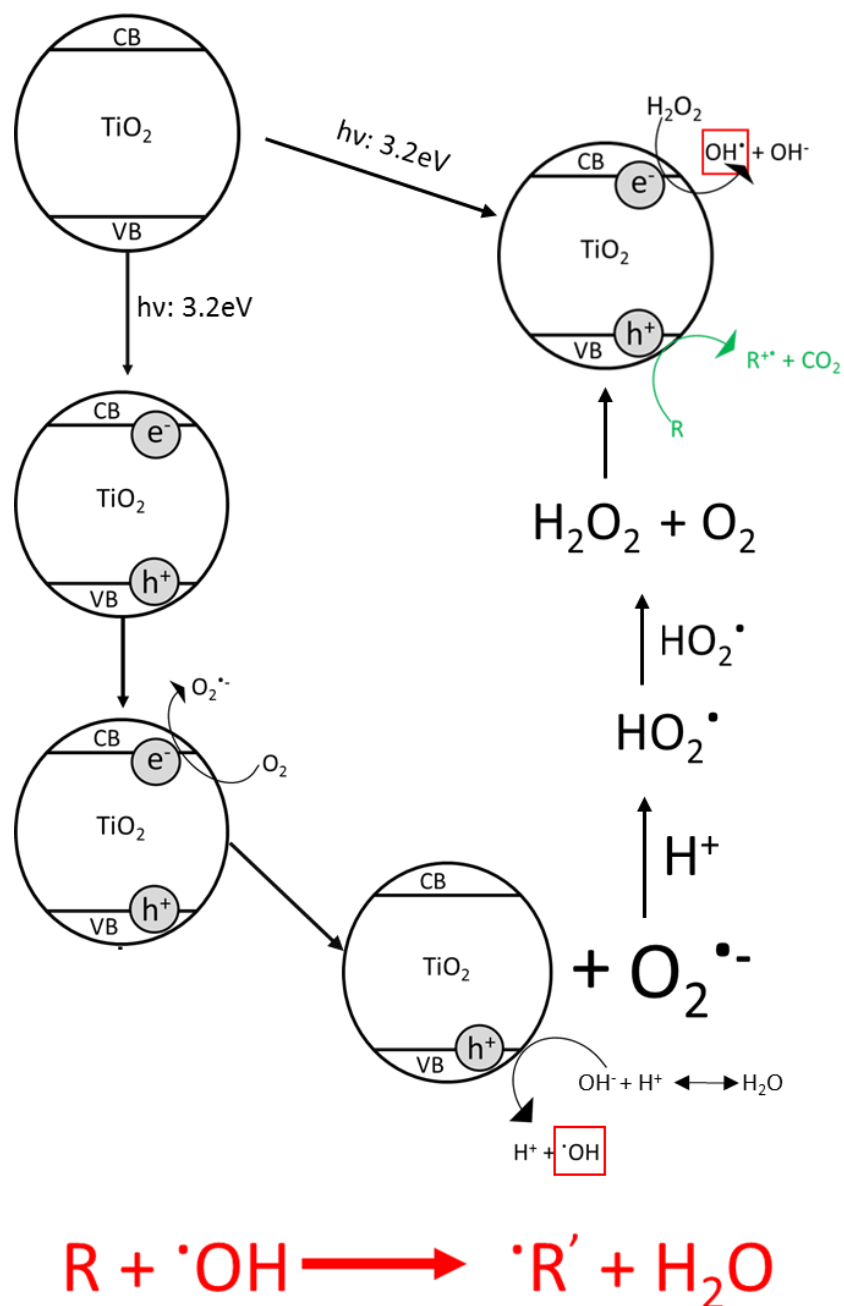


Figure 1.1: Photocatalytic degradation general mechanism. Each circle represents the TiO₂ photocatalyst. An electron is excited by a photon with 3.2 eV of energy from the valence band (VB) to the conduction band (CB) to generate an electron (e⁻) and electron hole (h⁺), which migrate to the surface. The electron and hole ultimately lead to the generation of hydroxide radicals (·OH) labeled with red boxes, which break down organic compounds by the general reaction colored red at the bottom of the figure. Direct oxidation of organic compounds via the electron hole also occurs, highlighted in the figure by a green color.

oxidation by holes contributes to degradation, the two processes occur concurrently. For the purposes of the current discussion, it is assumed that the organic compound is affected by both mechanisms. Figure 1.1 summarizes the general mechanism for the photocatalytic degradation of these types of compounds. Initially, a photon with a wavelength of 387 nm or less has sufficient energy (3.2eV) to excite an electron across the band gap of TiO₂ from the valence band to the conduction band. This leads to a charge separation referred to as an electron/electron-hole pair. In the next step, the electron of the charge-separated pair is used to reduce molecular oxygen to the superoxide radical (O₂^{•-}), and the electron hole charge neutralizes hydroxide ions via a one-electron oxidation to generate a hydroxyl radicals (OH[•]).¹⁶ Subsequently, the superoxide ion generated in a previous step begins a series of reactions, beginning with neutralization by a hydrogen ion (H⁺) to form a hydroperoxyl radical (HO₂[•]). Two molecules of the hydroperoxoyl radical then react to form one molecule of hydrogen peroxide and one molecule of molecular oxygen (by-product). A second excitation of TiO₂ regenerates the charge-separated pair. In this case, the electron is used for the decomposition of hydrogen peroxide into hydroxide ion (by-product) and another hydroxyl radical. The hydroxyl radicals formed during this process successively attack organic compounds to degrade them. At this point in the process, the electron hole is left on the TiO₂, and since it is electron poor it can then participate in the direct oxidation of adsorbed organic compounds.¹⁷

Although much is understood about the general process by which photocatalytic degradation acts, much less is understood about the intermediate products generated over the course of the degradation of specific compounds, especially those intermediate products which are short-lived.¹⁸⁻²⁰ This information is crucial due to the potential

formation of oxidation products which are more harmful than the initial compounds subjected to degradation. Many studies of photocatalytic degradation are exclusively kinetic in nature, focused mainly on the rate at which a particular chemical substance is removed by virtue of photocatalytic degradation, rather than the path by which it is removed. The main instrumental method used for these types of studies is ultra-violet and visible light source spectrophotometry (UV/VIS) which has the disadvantage of low chemical selectivity and thus is not particularly useful for assessing reaction mechanisms.²¹

1.3 Chromatographic Procedures (Traditional Analysis)

One of the most commonly used approaches to monitoring photocatalytic degradation reaction mechanisms involves gas or liquid chromatography coupled with mass spectrometry (GC/MS and LC/MS).^{18,22} Due to its high sensitivity and chemical selectivity, this is a powerful tool for the accurate determination of the structure of compounds present in a particular sample. To identify intermediate species occurring over the course of a reaction, small aliquots are taken from the reaction vessel at particular time intervals for analysis. Samples generally must be concentrated and dissolved in a specific solvent or carried by gaseous nitrogen in order to pass through a column, which is packed with material that will selectively interact with solutes. The degree of interaction between the column and the solutes determines the rate at which the solutes elute from the chromatography column.²³ Chromatography is coupled with analysis via mass spectrometry, which fragments molecules into ions and separates these ions based on their mass/charge ratio in order to identify species present in a particular sample.²⁴ Chromatography provides information regarding the structure of each solute, with a wide range of applicability since selective columns can be made to separate virtually any

chemical species, and concentration of solutes within a sample can be very low due to its high sensitivity.

In order to fully understand the advantages and limitations of traditional methods of analysis, it is useful to consider a specific example. In 2001, Houas and colleagues elucidated a portion of the reaction scheme for the photocatalytic degradation of methylene blue, a cationic organic dye.²⁵ Scheme 1.1 is adapted from the results found by this study. Analysis of total organic carbon (TOC) was used as an indicator for mineralization (breakdown to inorganic compounds such as CO₂) of methylene blue. Since the photocatalytic degradation of methylene blue ultimately results in the conversion of an organic carbon source (methylene blue) to an inorganic carbon source (CO₂), tracking a loss in TOC as a function of time allowed assessment of reaction rate. GC/MS and LC/MS was used to identify intermediate species arising over the course of the reaction. Chromatographic procedures coupled with mass spectrometry identify compounds with a high degree of certainty, which is important for accurate determination of reaction mechanism. However, as mentioned by the authors of this study done on methylene blue, although “many other hydroxylated intermediates were certainly formed” over the course of the reaction, they were unable to be detected either because they exhibited poor extractability due to hydrophilic character, or they existed for an insufficient period of time to analyze them by chromatographic procedures.

Despite its sensitivity and selectivity, chromatography has several disadvantages. Sample preparation is extensive and laborious, especially for LC/MS, in which the interaction between the column packing material and the solvent must be considered along with the interaction between the column material and the solutes.²³ Even for GC/MS,

wherein solvent interactions are not an issue, the selection of an appropriate column for a particular reaction is difficult and time consuming, and ideal conditions can even be different for various points in time over a single reaction. Additionally, these types of analyses are destructive; sample must be removed from the reaction vessel for analysis. Perhaps most importantly, data acquisition time is high, sometimes taking nearly an hour for analysis of a single sample.²² This is important because without data on a much shorter time-scale, intermediate species which are short-lived in the reaction can be missed, and thus an accurate reaction mechanism cannot be obtained.

1.4 Absorption Spectrophotometry/Spectroscopy

Chromatographic procedures are often coupled with spectroscopic methods, most commonly ultra-violet and visible light source (UV/VIS) spectrophotometry, in order to analyze reaction kinetics on a real-time scale.^{18,20,21} Although this technique is sensitive, it is not particularly selective due to its characteristically broad spectral features, and therefore peaks cannot be correlated well with particular changes in molecular structure, only overall analyte concentration. For this reason, determination of reaction mechanisms using UV/VIS spectrophotometry is difficult, especially for multi-component systems.

In UV/VIS spectrophotometry, photons from the ultra-violet and visible portion of the electromagnetic spectrum irradiate a sample, and the absorbance of photons as a result of electronic state transitions is measured. This limits the scope of applicability for these types of spectrophotometric procedures for reaction monitoring, because they require that the solution contains molecules which are able to undergo electronic excitations with energy corresponding to light in the UV/VIS range. Additionally, it is necessary to have a clear solution (which is not the case for samples containing TiO₂) since turbidity increases

scattering which would lead to artificially low detections of transmission (high absorption). Thus, limitations to UV/VIS spectrophotometry make it difficult to use for the purposes of analyzing photocatalytic degradation reaction mechanisms.

In contrast, vibrational spectroscopy provides high chemical selectivity. A commonly used form of vibrational spectroscopy is infrared (IR) spectroscopy. IR spectroscopy works in a very similar fashion to UV/VIS spectrophotometry, although the notable difference is that IR works over a different spectral range ($100\text{-}5000\text{ cm}^{-1}$) which corresponds to molecular vibrations rather than to electronic excitation. It is important to define some key terms used to describe properties of photons and electromagnetic waves at this time. Wavelength refers to the distance between crests of a wave, or distance per wave cycle, which is inversely proportional to the frequency of the wave, representing the number of cycles per unit time. Wavenumber is the mathematical inverse of wavelength, expressing the number of cycles per unit distance. The relationship between each of these terms is expressed as follows:

$$\tilde{\nu} = \frac{1}{\lambda} = \frac{\nu}{c}; \quad (1)$$

Where $\tilde{\nu}$ is wavenumber expressed in units of cm^{-1} , λ is wavelength in cm, ν is frequency in Hz (cycles per second) and c is the speed of light (3.00×10^{10} cm/s).

Both frequency and wavenumber are directly proportional to photon energy, which can be expressed as follows:

$$E = h\nu = h\tilde{\nu}c; \quad (2)$$

Where E is the energy of the photon in joules, ν is the frequency of the photon in meters, $\tilde{\nu}$ is the wavenumber of the photon in meters, c is the speed of light (3.00×10^8 m/s) and h is the Planck constant (6.63×10^{-34} J \times s).

IR photons have sufficient energy to induce an excitation from one vibrational energy state to a higher one via absorption. This process is quantized, such that only photons with the exact energy corresponding to a particular molecular vibration will be absorbed. Thus, by measuring absorbance as a function of wavenumber, molecular vibrations can be detected and used to infer details of molecular structure. IR spectroscopy is difficult to use for *in situ* monitoring of photocatalytic degradation in aqueous solutions due to strong signal associated with the molecular vibrations of water. The spectral feature associated with water absorption is broad, generally spanning over the 3200-3600 cm^{-1} range in an IR spectrum, while typical stretches are sharp (with narrow wavenumber ranges), such as the N-H stretch and the alkyne C-H stretch which appear at 3160-3240 cm^{-1} and 3280-3320 cm^{-1} respectively. Thus, water absorption would interfere with many stretches associated with analytes of interest.²⁶ Although it would be possible to dissolve analytes in an IR-inactive solvent to eliminate signal interference, this is not ideal because the established reaction pathway for photocatalytic degradation uses water directly to generate reactive oxygen species, which would not occur in alternative solvents. Additionally, since it relies on absorption measurements similar to UV/VIS spectrophotometry, IR spectroscopy is also generally ineffective for analysis of turbid media. Due to these limitations, this method might not contribute to the elucidation of intermediate products that could arise during wastewater treatment.

1.5 Project Goals: Expanding Applicability

Our approach to monitoring photocatalytic degradation uses Raman spectroscopy to monitor reactions *in situ* without extensive or destructive sample preparation. Raman spectroscopy provides the same chemical selectivity as IR spectroscopy, but without the

disadvantages of solvent interference and inability to assess turbid media. Reaction monitoring is accomplished via a flowing setup, and is advantageous mainly due to the speed of data acquisition, which is much faster than traditional methods and thus allows for short-lived intermediate species to be identified.¹⁹ This provides an effective complement to fill in the gaps in understanding left by analysis with traditional methods. Although this approach has shown effectiveness for highly soluble Raman-active compounds like iodinated contrast media (ICM), more work must be done in order to expand to other compounds of interest in wastewater treatment, such as the herbicides and pesticides. Along with introducing a means for acquiring quantitative information with regard to reaction kinetics, this project seeks to improve the sensitivity and reliability of the approach first described by Salkic, et al., to expand the applicability of Raman spectroscopy as a complementary analytical tool for better understanding reaction mechanisms underlying photocatalytic degradation of wastewater pollutants.¹⁹

1.6 Compounds of Interest

Our lab has previously studied the photocatalytic degradation of ICM, and this work seeks to expand the scope of our methods to other harmful pollutants.¹⁹ Among the most interesting compounds for our purposes are ionic and ionizable pesticides and herbicides. Some examples of herbicides considered for study in our lab are depicted in Chart 1.1, including bentazon (1), atrazine (2), and 2-methyl-4-chlorophenoxyacetic acid (3). These compounds are termed “ionizable” because they can be protonated or deprotonated as a function of pH such that they will then have a positive or negative net charge, respectively.²⁷ Some herbicides are ionic, present as chloride or bromide salts which

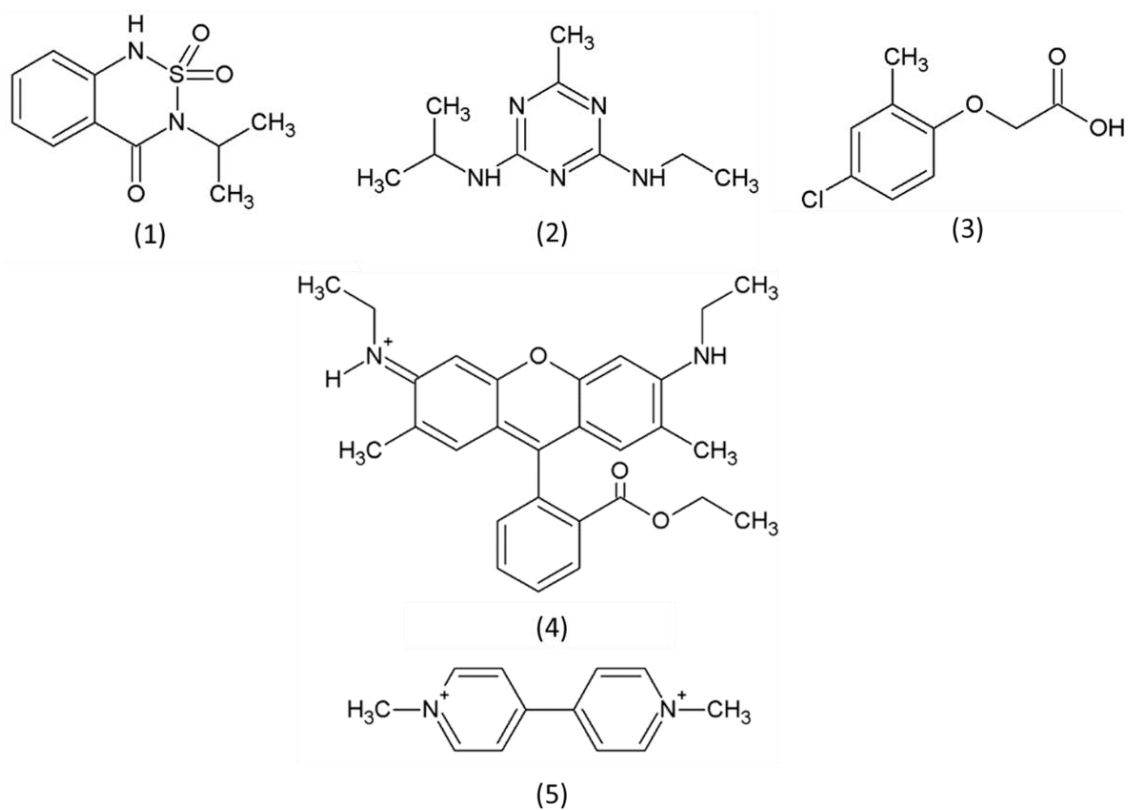


Chart 1.1: Structures for compounds of interest. 1) bentazon 2) atrazine 3) MCPA 4) rhodamine 6G (R6G) and 5) paraquat. Bentazon, atrazine, and 2-methyl-4-chlorophenoxyacetic acid (MCPA) are ionizable herbicides. R6G and paraquat are cationic organic compounds studied in this work. R6G is a dye used as a test molecule for our purposes, and paraquat is a common herbicide.

readily dissociate in aqueous solution regardless of pH. Some examples of these include paraquat, diquat, difenzoquat, chlormequat, and mepiquat.²⁸

Since the majority of data collected to date for this project has focused on cationic species such as paraquat and rhodamine 6G (R6G), it is useful to discuss them in some detail prior to moving forward. The structures of R6G and paraquat are depicted in Chart 1.1 (4-5). R6G is a cationic organic dye which is used in a variety of contexts. Although it is probably most well-known for its fluorescent properties, R6G is a commonly used test molecule for studies involving surface-enhanced Raman spectroscopy because its cationic nature and inherent polarizability allow it to be subjected to high degrees of electromagnetic and chemical Raman scattering enhancement (discussed in more detail in Sections 2.1-2.3). Since R6G is an organic halide salt, studying its photocatalytic degradation can be used to develop methods of analysis which can be applied to other molecules of this type which are more relevant to wastewater treatment. Paraquat, also known as methyl viologen, gramoxome, and zeneca, is an herbicide which acts by disrupting electron transfer in enzymes involved in photosynthesis.²⁹ Since it is an oxidant, paraquat is able to readily accept electrons and subsequently transfer them to molecular oxygen to generate reactive oxygen species (such as the superoxide ion, $O_2^{\cdot-}$) that kill cells when present in large amounts. Although it is effective as an herbicide, it has the disadvantage of low reactive selectivity, meaning it can accept electrons from a variety of different compounds for use in generating reactive oxygen species.³⁰ Since electron transfer is a basic method which nearly all organisms use in some capacity to generate cellular energy, paraquat can have toxic effects on most living organisms. In humans, exposure to paraquat has been linked to both severe physical symptoms associated with

acute toxicity and long-term effects of increased likelihood to develop neurodegenerative disorders such as Parkinson's disease.^{31,32} Thus, removal of paraquat from agricultural farm runoff with simple methods like photocatalytic degradation is thus highly desirable.

CHAPTER 2

Experimental Methods: Tools for Monitoring Photocatalytic Degradation

The approach to monitoring photocatalytic reactions discussed in this thesis offers several advantages over traditional methods, and thus will be a useful complimentary tool capable of obtaining information beyond that which is possible by current approaches. This chapter provides necessary background information for understanding the reasoning behind experimental designs, the methods by which data are retrieved, and important procedural steps for relevant experiments.

2.1 Raman Scattering

In light scattering, a photon is never absorbed by a molecule. There are two general types of photon scattering: elastic (Rayleigh) and inelastic (Raman) scattering. The simplified general Jablonski energy level diagram depicted in Figure 2.1 illustrates Stokes and anti-Stokes Raman scattering, as compared to elastic Rayleigh scattering. Although it is not technically accurate, it is useful to visualize scattered photons as simply particles colliding with a stationary vibrating molecule. If the collision between the photon and the molecule is elastic, the photon is scattered without experiencing a change in energy. This type of scattering is known as Rayleigh scattering. Raman scattering differs from Rayleigh scattering because it is inelastic, meaning the photon experiences a change in energy as it is scattered. This energy shift yields a scattered photon of higher energy if energy is transferred from the molecule to the photon (anti-Stokes scattering) or lower energy if

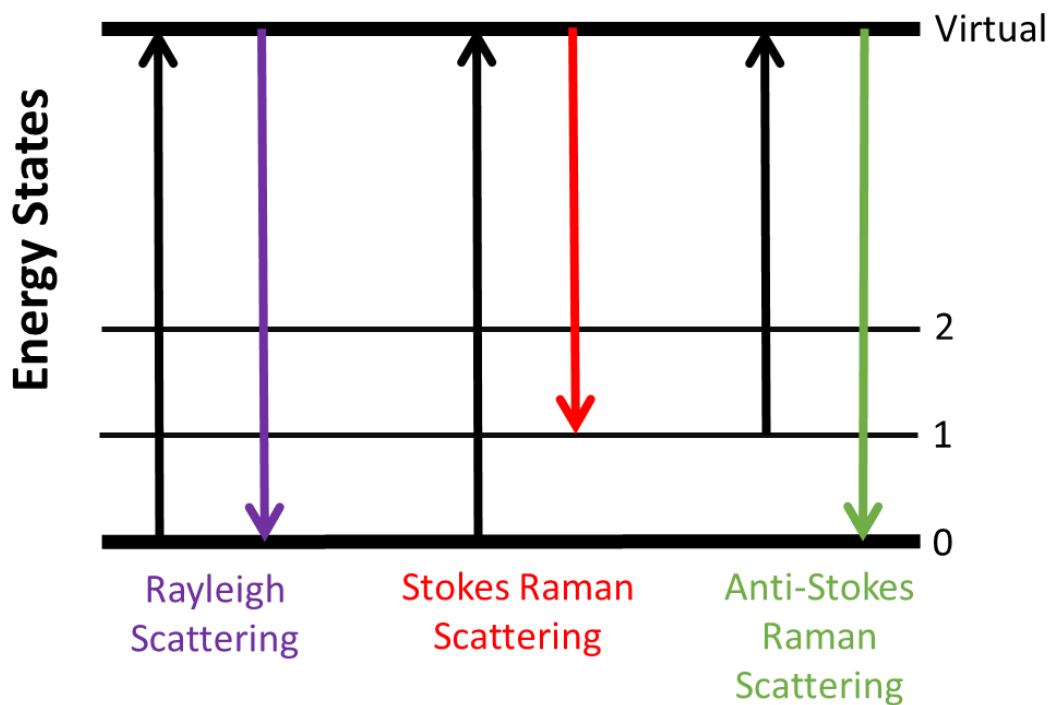


Figure 2.1: Scattering: Jablonski energy level diagram. A comparison of the effect of various types of photon scattering on photon energy. In each case, a black arrow indicates an incident photon, whereas colored arrows represent the resulting scattered photon. A photon can be scattered elastically with no change in energy (Rayleigh scattering, purple), less energy than initially (Stokes Raman scattering, red), or greater energy than initially (anti-Stokes Raman scattering, green). To account for the energy shift experienced by the photon, this model considers the scattering process as though it involved an excitation to a non-existent energy state (labeled virtual) with subsequent emission. Energy states labeled 1 and 2 correspond to vibrationally excited energy states, and the energy state labeled 0 is the lowest vibrational state associated with a particular electronic energy state.

energy is transferred from the photon to the molecule (Stokes scattering). The amount of energy by which a photon shifts is equal to the energy associated with the corresponding molecular vibration.³³ In most cases, molecules in solution are in the ground vibrational state (the lowest energy vibrational state within the lowest energy electronic state) prior to excitation with a laser. For this reason, Stokes scattering is more common than anti-Stokes. Inelastic scattering is a scarce effect, and as a result Rayleigh scattering is one million times more probable than Raman scattering.

2.2 Raman Spectroscopy

Raman spectroscopy is often used as a form of vibrational spectroscopy which relies on the inelastic scattering of photons caused by molecular vibrations.³⁴ Since the vibrational modes associated with a molecule are indicative of structural features, knowledge about the energy shift experienced by photons irradiating a sample can be used to deduce information regarding molecular structure. Figure 2.2 depicts a block diagram of the R3000 Raman system setup used in this work. This system uses a 785-nm laser to irradiate samples, and detects back-scattered photons to minimize background noise which would be associated with transmission. A Raman spectrum plots the “count” of photons detected as Raman intensity, as a function of the shift in energy experienced by the detected photons known as Raman shift, expressed in terms of wavenumber. Wavenumber is most commonly measured in units of inverse centimeters, while Raman intensity has arbitrary scaling which is related to the relative number of photons of a particular energy shift reaching the detector. Raman shift is calculated by comparing the wavenumber of the incident photons with the wavenumber of scattered photons. Aqueous Raman spectra, which constitute the majority of data collected in this work, use a “liquid” tip on the Raman

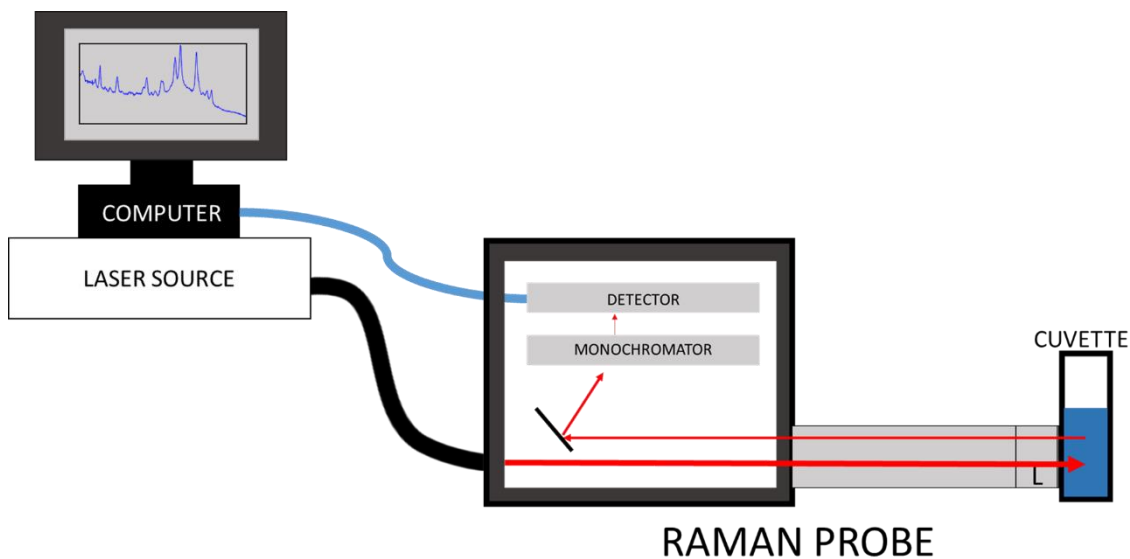


Figure 2.2: Block diagram of Raman system. In the R3000 Raman system, 785-nm laser source emits monochromatic light through the probe and into the sample; this light is represented by the red arrows. The probe is shown with a “liquid” tip, labeled L, which focuses light appropriately for measurements of liquid samples in a cuvette. A shorter “solid” tip is used for powder Raman spectra. The returning photons travel through a monochromator which separates them based on their wavelength. The count of photons at a particular wavelength is relayed by the detector to a computer, which translates wavelength of photons to Raman shift relative to incident photons. RSIQ computing software then generates a plot of Raman intensity as a function of energy expressed in terms of wavenumbers, which have units of inverse centimeters.

probe such that the focal point of the laser is several millimeters in front of the probe head, and thus data points are collected at a point within the liquid solution in a cuvette. These measurements use 300-mW laser power, and an integration time of 10 s. For powder samples, a “solid” tip is employed which focuses the laser immediately beyond the edge of the probe. Integration times associated with powder samples also use a laser power of 300 mW, but with an integration time between 2 s and 4 s.

To demonstrate the correlation of spectral features in a Raman spectrum with molecular structure, Figure 2.3 uses a spectrum of a 1 M solution of potassium nitrate (KNO_3) as an illustrative example. The nitrate ion exhibits a single spectral peak at 1050 cm^{-1} , which corresponds to the molecular vibration (symmetric stretch) illustrated in the Figure 2.3(a).³⁵ Coupled with computational analysis of the expected vibrational modes for a particular analyte, structural information can be deduced from spectral features.^{19,36}

Raman spectroscopy is just as selective as IR spectroscopy, but it does not have the same disadvantages. Raman-active vibrational modes associated with water exhibit very weak spectral intensity, and thus spectra can be measured of aqueous solutions without interference from the solvent. Additionally, Raman spectroscopy is not affected by turbid media. The Raman system detects back-scattered photons: the only ones recorded are those which are shifted in energy relative to that of the photons emitted from the laser. Therefore, elastically scattered photons do not contribute to background noise as long as they are sufficiently separated in wavenumber from Rayleigh scattered photons. Raman spectroscopy is advantageous over traditional chromatographic procedures because data points can be acquired *in-situ*, and data acquisition takes only seconds rather than minutes. This allows for identification of some structural features of intermediate species which may

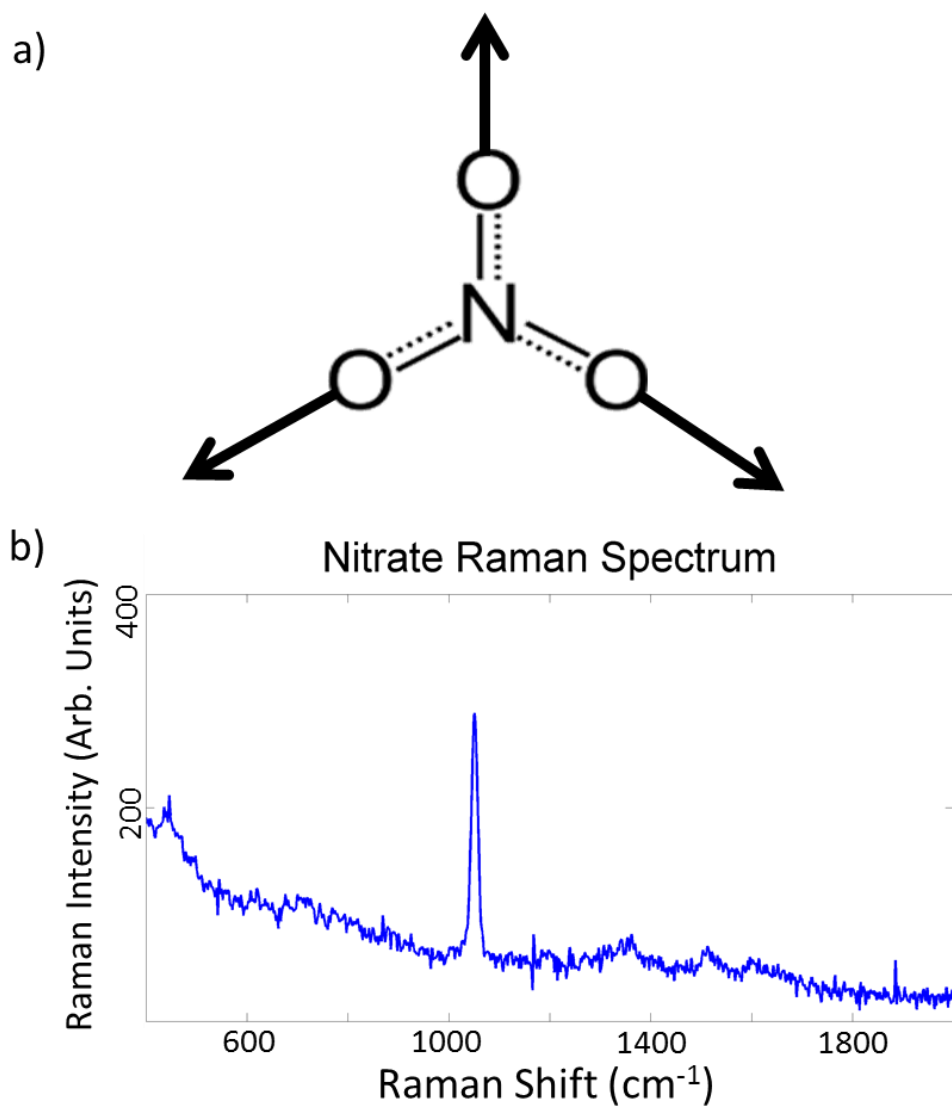


Figure 2.3: Raman nitrate ion example. a) the Raman active vibrational mode associated with the nitrate ion is a symmetric stretching of the three oxygen atoms outward from the central nitrogen atom. Molecular vibrations of this type are often described by comparing the atoms to masses on the ends of an oscillating spring. b) the Raman spectrum of aqueous 1-M potassium nitrate solution plots Raman intensity as a function of Raman shift, which is directly proportional to the energy shift experienced by the scattered photons. The peak exhibited in the curve at 1050 cm^{-1} corresponds to the shift in energy experienced by photons as a result of energy transferred to the molecule from the photon as a result of this scattering, since the plot shown here includes the detected spectrum for Stokes-shifted photons.

be missed by traditional forms of analysis. Another project in the Nee lab is focused on developing a nanosecond pulsed laser for later Raman studies which will allow even faster data acquisition (multiple spectra per second) once optimized.

2.3 Surface Enhanced Raman Spectroscopy

Although the use of Raman spectroscopy as a complementary approach offers several advantages, there are disadvantages in its practical use for monitoring reactions. One such disadvantage, especially in the context of wastewater treatment, is that many analytes are not sufficiently soluble to generate concentrations high enough for data acquisition using Raman spectroscopy. However, the sensitivity of Raman spectroscopy can be increased 10^8 fold via surface enhancement.³⁷ Surface-enhanced Raman spectroscopy (SERS) refers to the use of roughened metal surfaces or colloidal nanoparticle suspensions to increase Raman signal intensity.^{37,38} Although the exact mechanism resulting in SERS is not entirely understood, it is well established that oscillations of electrons (plasmons) on a roughened metal surface or asymmetric nanoparticle cluster generates a local electric field when excited by photons of an appropriate wavelength from a laser. Excitation of a plasmon promotes energy transfer to an adsorbed molecule, and initiates the Raman process. The energy transferred back to the plasmon is then less than the energy which originally left it due to transfer to the molecule, and thus scattered photons from the plasmon are shifted in energy.^{38,39} This explanation, known as electromagnetic enhancement, does not account for the full magnitude of enhancement exhibited in many cases.^{40,41} In order to account for the additional observed enhancement, the less-understood chemical enhancement hypothesis has been proposed, which involves the effect of strong adsorption of the analyte, enhancing polarizability.^{39,42} Polarizability is important to

inducing Raman scattering: more polarizable compounds are more Raman active.⁴³ It is important to note that chemical and electromagnetic enhancement do not act independently, but rather act simultaneously to enhance Raman signal.^{37,42,43}

SERS is potentially widely applicable, but to date it has mainly been used for the detection of molecules rather than monitoring their changes as a function of time. SERS has been used in the contexts of single-molecule detection,⁴⁴ detecting presence of particular compounds in living cells,^{45,46} detecting modified estrogens,⁴⁷ environmentally harmful substances,⁴⁸ and many others. While it is a powerful tool for sensitive detection of analyte in a given sample, it does have some limitations associated with long-term reaction monitoring, as discussed in more detail in Sections 2.6 and 2.7. One of the goals of the current work is to resolve these issues.

In the context of the current work, SERS involves the adsorption of analytes onto colloidal gold nanoparticle clusters, the properties of which will be discussed in Sections 2.4-2.6. After adsorption of analyte to the nanoparticle surface, data are acquired using the Raman system in the same way as any other sample. Although modification of nanoparticles is often necessary for effective SERS, especially when multiple spectra are to be taken over a period of time, sample preparation always involves adsorption of analyte onto nanoparticles or clusters of nanoparticles prior to data acquisition.

2.4 Nanoparticle Synthesis

Nanoparticles are synthesized by a citrate reduction procedure adapted from a paper published by Lee and Meisel in 1985.⁴⁹ Figure 2.4 illustrates the nanoparticle synthesis setup with a photograph taken in lab which labels relevant components. First, 120 mg of chloroauric acid (HAuCl_4) is dissolved in 250 mL of deionized water in a round-bottomed

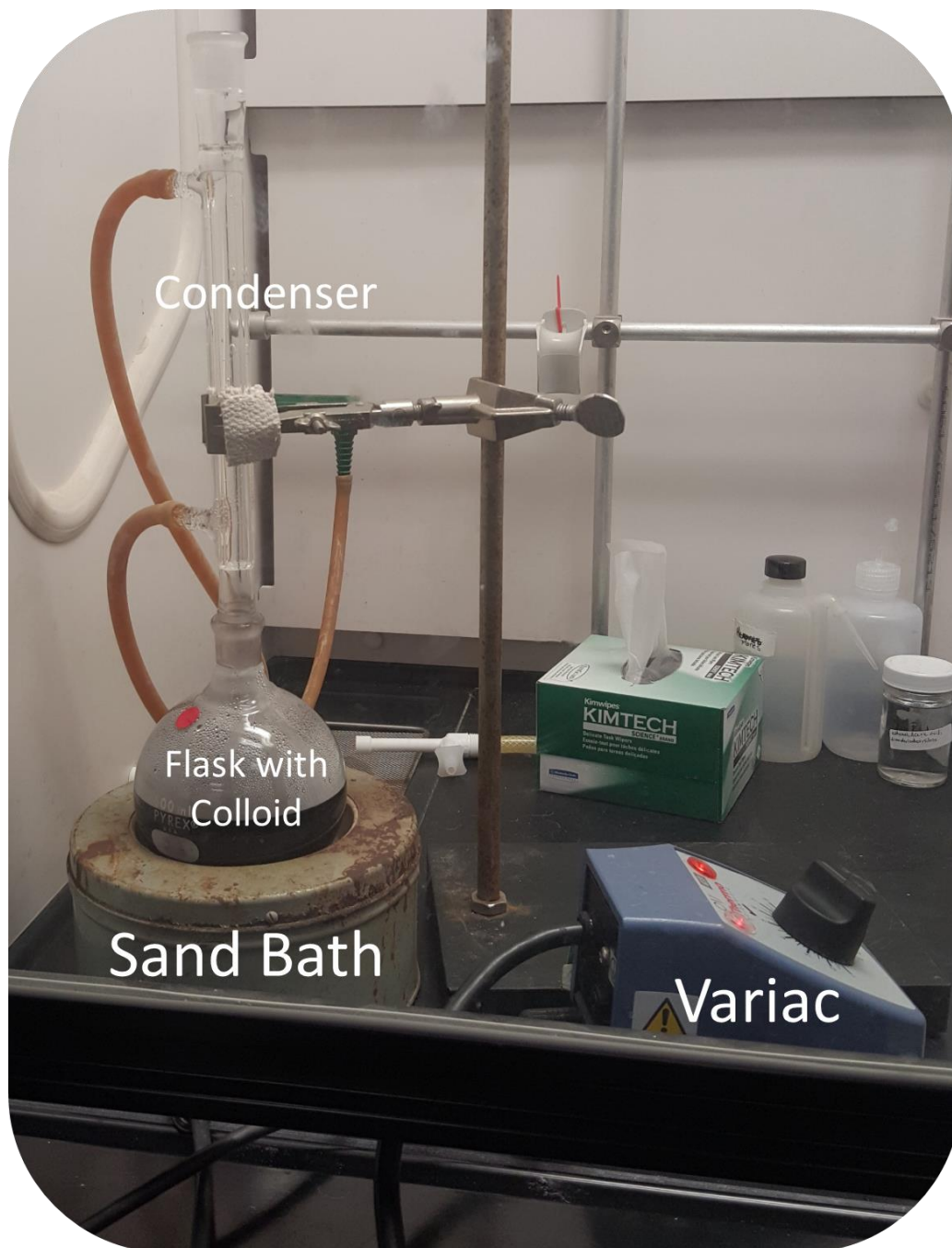


Figure 2.4: Nanoparticle synthesis. Setup for the synthesis of colloidal gold nanoparticles by standard citrate reduction. HAuCl_4 dissolved in water is brought to a boil in a round-bottomed flask using a sand bath, employing a variac for temperature regulation. Once boiling, 1% sodium citrate is added to reduce gold to its uncharged state. A condenser is placed over the flask, stabilized by a clamp on an adjacent ring stand. Water in the condenser prevents evaporation of the water in the nanoparticle colloid. The solution is allowed to boil for one hour.

flask, producing a yellow solution, which is brought to a boil using a sand bath. Once boiling, 25 mL of 1% aqueous sodium citrate ($\text{Na}_3\text{C}_6\text{H}_5\text{O}_7$) solution is added, and a condenser is placed over the top of the round-bottomed flask to prevent evaporation during the subsequent 1-hr boiling period. Upon initial addition of sodium citrate, the solution becomes colorless. Shortly thereafter, the solution changes to a dark purple, and finally to a maroon-red towards the end of the process. The net result is a reduction of gold atoms to an oxidation state of zero via citrate and subsequent capping with citrate as well to form a colloidal suspension stabilized by electrostatic interactions between ions present in the aqueous solution surrounding the nanoparticles.

2.5 Nanoparticle Characterization

Initial colloidal gold nanoparticle characterization involves acquisition of an absorption spectrum in the UV/VIS range. Since UV/VIS spectrophotometry is responsive to electronic transitions in a molecule or particle within a solution, it is useful for detection of the excitation wavelength associated with the surface plasmon resonance of nanoparticles and nanoparticle clusters. A UV/VIS absorption spectrum is a plot of absorbance as a function of wavelength. The peak of the curve represents the wavelength most frequently absorbed, which indicates the surface plasmon resonance excitation energy of the nanoparticles. Ideal maximum absorption should be near (but not overlapping) the energy associated with the emitted wavelength of the laser at 785 nm. Overlap could result in fluorescence of the nanoparticles, which would interfere with signal for a back-scatter Raman detector since fluorescence, like scattering, occurs in all directions. In fact, optimal absorption contributed to the decision to use colloidal gold nanoparticles over other SERS substrates, since they exhibit surface plasmon resonance with appropriate excitation

energy.^{50,51} It should also be noted that initially, colloidal silver nanoparticles were used, but the lack of success in producing SERS signal using compounds other than R6G, such as the selected internal standard carbon disulfide (CS₂), also contributed to a shift toward colloidal gold nanoparticle synthesis.

The wavelength of maximum absorption determined from UV/VIS spectrophotometry indicates the presence of surface plasmon resonance, a property which correlates strongly with nanoparticle size. It is useful to consider the two-dimensional “particle in a box” model often referenced in the context of quantum mechanics. Figure 2.5 illustrates this model, which considers the nanoparticles as a “box” and an electron as a particle which can only exist between the walls of the box because the potential energy outside of the box is infinite, and the potential energy between the walls is zero. Thus, the particle is confined to the region inside of the box. Energy levels in the model determine the 0 value for various wave functions, which predict the probability of an electron’s presence at points along the axis. Solving the Schrodinger equation given the parameters associated with this model for energy at a given quantum number yields:

$$E_n = \frac{n^2 h^2}{8mL^2} \quad (3)$$

Where E_n is the energy associated with a particular electronic transition, n is the principle quantum number (1, 2, 3...), h is the plank constant (6.6×10^{-34} J×s), m is the mass of the particle in kilograms, usually an electron, and L is the length of the box in meters, representing nanoparticle size for our purposes.

Equation 3 shows that as the length of the box decreases, the energy associated with each electronic transition will increase. Therefore, smaller nanoparticles will require higher energy (lower wavelength) electromagnetic radiation to induce an electronic excitation

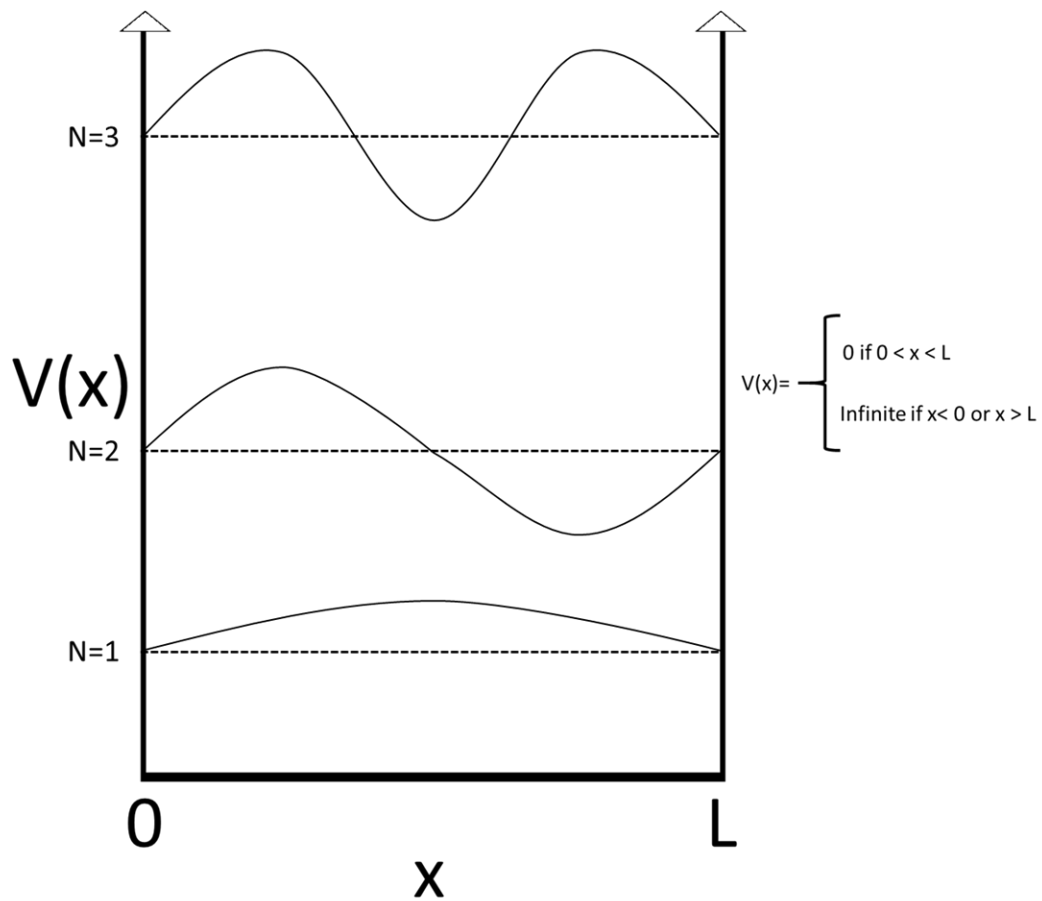


Figure 2.5: Particle in a box. For a two-dimensional particle in a box, the particle must exist at some point between its initial position 0, and a final position designated L. The distance from 0 to L is the length of the box, and x defines all of the possible positions along the length of the box at which the particle can be. $V(x)$ is the potential energy of the particle. Wavefunctions depicted at various energy states (N) indicate the probability of the particle to be present at a particular position (x).

than larger nanoparticles, which is reflected by the maximum absorbance in UV/VIS spectrophotometry.

Although UV/VIS spectrophotometry can provide some indication of average nanoparticle size, information regarding the shape and size distribution of the nanoparticle suspensions require high-resolution imaging techniques. Transmission electron microscopy (TEM) is an imaging technique which in many ways acts according to principles similar to general light-field microscopy. However, a beam of electrons is used rather than a form of electromagnetic radiation in order to yield a 200-fold increase in resolving power.⁵² Contrast is generated via repulsion of electrons by electron-dense heavy metals. Although sample preparation is often quite extensive, especially in the context of biological samples which must be doped with heavy metals, images of colloidal gold nanoparticles can be taken with little sample preparation since their cores are already highly electron dense. A drop of nanoparticle colloid was placed onto a copper-coated grid and treated with fixing agents which helped to adsorb the nanoparticles onto the grids to promote dispersion over stacking, so that nanoparticle size could be accurately determined. After adsorption to the copper grid, excess fixing agents were gently rinsed away, and the nanoparticle-attached grids were allowed to dry for a period of 48 hours. Once dried, the nanoparticles were imaged using the JEOL 100CX microscope in the WKU TEM facility.

Once images were collected using the TEM, the determination of nanoparticle diameter involved several steps. First, an appropriate image was chosen which had a large number of nanoparticles visible in it, without interference from many sample impurities or unusually large aggregates. Next, since scaling reported by the instrument is not entirely reliable, the scale was corrected by analyzing a grid which contained a diffraction grating

of known groove separation. Scale correction allowed for accurate determination of the relationship between the distance reported on the scale bar and the true distance across which the images spanned. Once an accurate scale was established, the chosen image was edited using Photoshop. The image was converted from grayscale to pure black/white, and contrast was altered such that nanoparticles in the figure appeared as white patches on a black background. The image was also edited at the edges such that sectioned nanoparticles would not be recognized as full nanoparticles which were smaller in size. Since the nanoparticles were roughly spherical, the white patches were fit to circular templates, and the diameter of these fit circles represented an estimate for nanoparticle diameter. The generated comma separated value (.csv) file readable in Microsoft Excel reported the count of each recognized circular patch along with its associated diameter in pixels. The original scale bar was fit to its rectangular shape and the length was determined in terms of pixel number. Thus, a direct correlation between pixel number and true length was made, and used to create a new column in the Excel spreadsheet indicative of the diameter of the nanoparticles in nanometers. The Excel program was then used to generate a frequency distribution chart which illustrates the number of nanoparticles of several chosen size ranges in the form of a bar graph.

2.6 Colloidal Aggregation

When an electrolyte is introduced into a colloidal suspension, the effect of crystal growth is favored over nucleation.⁵³ In the context of colloidal gold nanoparticles, “crystal growth” manifests as aggregation; the combination of individual nanoparticle cores into a larger nanoparticle cluster. Nanoparticle aggregation is important to surface enhancement.⁵⁴⁻⁵⁷ As mentioned in Section 2.3, SERS requires a roughened metal surface

or nanoparticle cluster. Since the nanoparticles synthesized by the citrate reduction method are essentially spherical, aggregation is necessary to provide an appropriate roughening in order to entrap analyte molecules into a SERS “hot spot” in which signal can be enhanced by adjacent nanoparticles.^{51,57} SERS is only possible if aggregation happens after or simultaneously with addition of analyte, since aggregation of colloidal nanoparticles prior to analyte addition closes off these “hot spots” which lie on the interior of nanoparticle clusters. Simultaneous addition of electrolyte and analyte is employed for these experiments. For organic salts such as R6G and paraquat, the analytes are themselves electrolytes. For other species, such as the internal standard CS₂, it is necessary to add electrolyte such as sodium chloride simultaneously in order to observe any SERS spectrum.

2.7 Secondary Capping

Since SERS is typically used as a qualitative detection technique, nanoparticle stabilization is not often an issue of concern. Stability over time becomes important for the purposes of the current work, however, because nanoparticles are not stable enough to monitor reactions over an extended period. Although much work has been done to make metallic nanoparticles which are highly stable to changes in pH, electrolyte concentration, and stirring, most of these nanoparticle synthesis procedures are not useful for our purposes.^{59–62} They tend to make small, spherical, monodispersed nanoparticles which are useful in many contexts, but have several disadvantages for use in reaction monitoring via SERS. First, the most common highly stable nanoparticles are not within the size range appropriate to generate surface plasmon resonance with an excitation energy appropriate for our purposes.^{61,63} Additionally, many of them are ultra-stable due to the fact that they allow for no aggregation, with bulky capping agents stabilizing the nanoparticles by not

allowing them to come into proximity with one another or added electrolyte molecules.^{59,62} These types of particles would not allow binding of the analyte for use in SERS, or the formation of roughened nanoparticle clusters, and may even inhibit reaction of analytes.

Displacing the citrate capping agent of gold nanoparticles with another molecule can help to increase nanoparticle stability. Most commonly, sulfhydryl-terminated organic compounds are used for the purposes of displacing citrate molecules, since these groups are reactive enough to interact more strongly with the nanoparticle core than the oxygen atoms of citrate. Mid-length thiolated alkanes such as 1-decanethiol are commonly used to displace citrate from citrate-capped gold nanoparticle cores. Full displacement is useful for generation of nanoparticles which have a diameter range of 3-5 nm, but this size of nanoparticle is not effective for surface enhancement.⁶⁴ However, it is important to note that 1-decanethiol has been used in stabilizing SERS substrates previously: it was used to stabilize solid acid-etched SERS substrates, in which nanoparticles are fixed into a monolayer and roughened by a manual etching procedure. For these types of substrates, stabilization is not used to prevent nanoparticle aggregation, but rather to prevent breakdown of the SERS substrates under storage conditions due to air, light, water, etc.^{65,66} These SERS substrates are stable and sensitive, but they are more applicable to use in sensitive detection of solutes in a particular solution than to reaction monitoring, since solid SERS substrates have a fixed location and thus cannot be dispersed throughout a reaction vessel. Stabilized nanoparticles are advantageous for reaction monitoring because they allow monitoring in-situ without signal diminishment as a consequence of nanoparticle aggregation. The maintenance of signal constancy is crucial for gaining reliable information regarding reaction kinetics.

Figure 2.6 illustrates secondary capping with 1-decanethiol. If 1-decanethiol is present in dilute amounts such that nanoparticles maintain their size and an ability to aggregate to a certain extent, these semi-aggregated nanoparticle clusters can be secondarily capped by 1-decanethiol to provide a layer of steric stabilization and maintain cluster size over an extended period of time. If too much secondary capping agent is present, the citrate capping agent is fully displaced and the nanoparticles will decrease significantly in diameter. Upon subsequent addition of analyte, these small nanoparticles are ineffective at producing SERS signal. However, if the concentration of capping agent is sufficiently low, it will not be effective at displacing citrate ions until the surface area of the nanoparticles is sufficiently lowered by their aggregation. Once the nanoparticles are semi-aggregated, some citrate molecules can then be displaced by the 1-decanethiol molecules and have a stabilizing effect on the nanoparticle clusters. We have not seen evidence of previous secondary capping of nanoparticles for use in surface-enhanced Raman spectroscopy, suggesting that this is a novel approach for maintaining spectral signal over time which allows for effective reaction monitoring *in situ*.

1-decanethiol is highly insoluble in water. Volumes of 1-decanethiol which are measureable by equipment in our lab are too high to place into any reasonable (25 mL or less) sample volume of colloidal nanoparticles without exceeding the concentration that fully displaces citrate. For this reason, the secondary capping agent is introduced by pipetting one drop of 1-decanethiol into a flask, and then rinsing this flask five times with deionized water, after which 25 mL of a colloidal gold nanoparticle suspension are added and placed on a constant stir until an analyte is added.

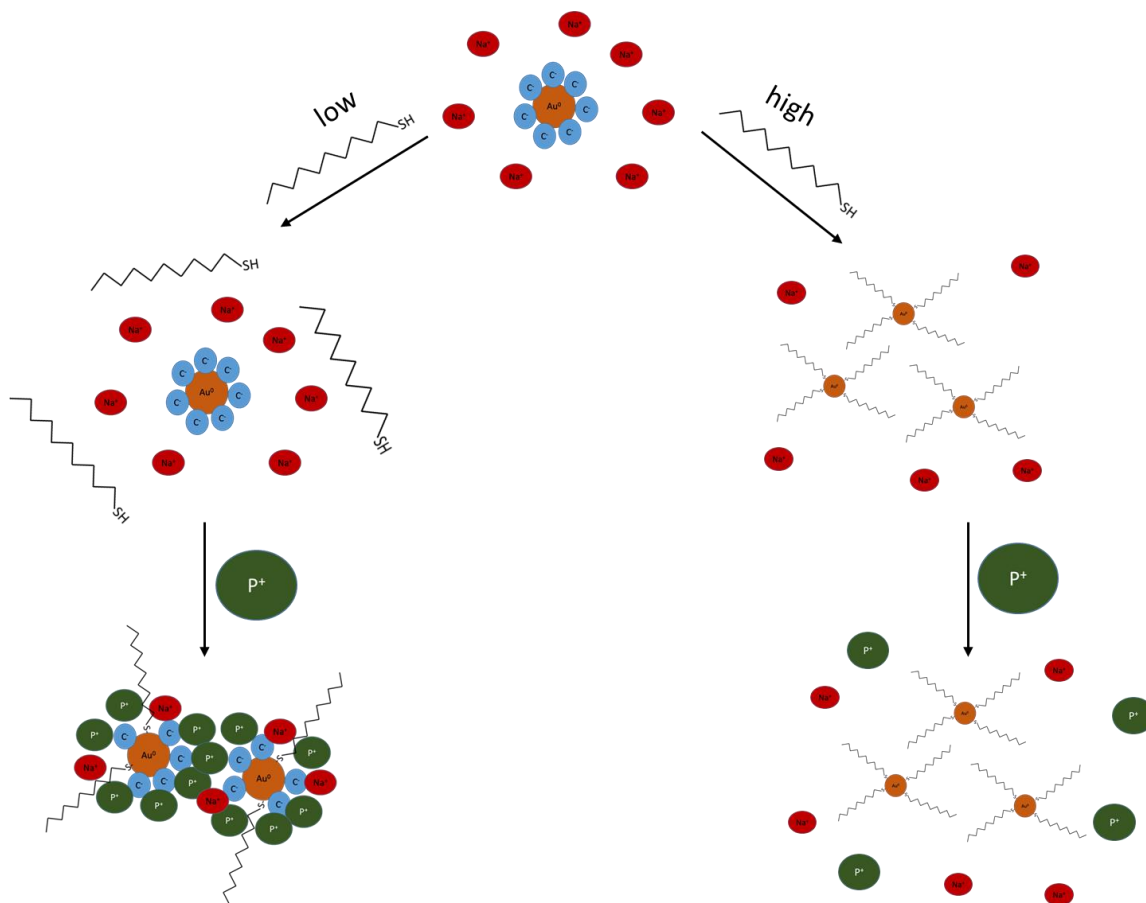


Figure 2.6: Nanoparticle stabilization via decanethiol. Nanoparticles exposed to 1-decanethiol represented by the zig-zagged line interact differently based on 1-decanethiol concentration. Nanoparticles exposed to a low concentration of 1-decanethiol do not experience full displacement of citrate, and thus nanoparticle clusters are stabilized. Nanoparticles exposed to excess 1-decanethiol experience full displacement of citrate, which results in smaller nanoparticle cores that are then ineffective at adsorbing analyte onto the nanoparticle surface. In this diagram, Au⁰ represents the nanoparticle core, C⁻ represents the citrate capping agent, Na⁺ represents sodium ions, P⁺ represents paraquat.

2.8 Calibration Curve Generation

With sufficiently stabilized nanoparticles for surface enhancement, it is possible to monitor a reaction involving attainable analyte concentrations for long enough to gain qualitative information useful in identifying intermediate species important to reaction mechanisms. However, another limitation of Raman spectroscopy is the inability to generate reliable information with regard to analyte concentration based on spectral data/Raman intensity values, which are reported in arbitrary units and can vary significantly from spectrum to spectrum of a single solution due to inherent variabilities. Even though the specific intensities vary, the ratio of one peak relative to another within the spectrum of a particular solution is expected to remain the same regardless of variability in the specific values. An internal standard can be added as a point of reference.^{67,68} Many groups use solvents as the internal standard for Raman experiments,⁶⁹⁻⁷² which is not feasible for our purposes since the solvent here is water, which does not exhibit vibrational modes in a Raman spectrum with sufficient intensity to be compared with other spectral features. Quantitative SERS has also been shown using self-assembled monolayers (SAM) on solid SERS substrates, but such substrates are more useful for determination of concentration in a solution for the purposes of detection, rather than monitoring change in analyte concentration as a function of time.⁶⁷

The internal standard selected for our purposes was carbon disulfide (CS₂). Even though internal standards in Raman studies are widely used, the use of CS₂ as an internal standard, to our knowledge, is novel, and provides advantages over more commonly used internal standards for photocatalytic reaction monitoring. Carbon disulfide meets several important criteria to qualify it for effective use as an internal standard. It is Raman-active,

and only exhibits a single stretch at 650 cm^{-1} over the range of wavenumbers examined by our Raman system. A simple Raman spectrum minimizes signal overlap, and thus allows accurate differentiation between the peak associated with the internal standard, and those of analytes. Additionally, carbon disulfide is not expected to be subject to photocatalytic degradation, such that its concentration can remain constant over the course of a monitored reaction. Although CS_2 is not particularly soluble in water, it is sufficiently soluble to allow for a SERS spectrum to be taken in the presence of semi-aggregated gold nanoparticle clusters.

In general, calibration curves allow for the determination of analyte concentration based on analysis of the features of several known solutions containing this analyte to develop a general trend. Here, a calibration curve develops the relationship between analyte concentration and Raman spectral features. More specifically, the spectral features involved are ratios between the intensity of analyte peaks and that of the peak associated with the internal standard. If the concentration of internal standard is kept constant, then it is expected that the intensity of analyte peaks relative to the peak of the internal standard will be higher when the concentration of analyte is high, and lower when analyte concentration is low. Therefore, making solutions of nanoparticles which have a constant concentration of internal standard and introducing a different concentration of analyte into each solution allows for a calibration curve to be generated.

“Intensity” in this case does not refer to the peak value of Raman intensity associated with various stretches in a spectrum. Rather, peaks are fit to Gaussian curves, and the integrated area under these curves is calculated to determine a value for intensity. For spectral peaks which overlap, we are able to specify this such that two Gaussian curves

are fit simultaneously, correcting for error that would otherwise be associated with the fitting parameters. Using areas under curves fit to specific stretches is preferable because it more accurately determines relationships between spectral features and analyte concentration. It also allows for monitoring changes that are not necessarily associated with changes in peak height, such as broadening of peaks within a spectrum as a result of some structural change caused by a reaction.

For the preliminary calibration curves generated in this work, carbon disulfide was added at a concentration of 2% volume per volume (V/V) in each case, and the analyte rhodamine 6G was then added. The first generated calibration curve covered a concentration range of R6G from 2×10^{-5} M to 1×10^{-4} M. The second calibration curve generated with uncapped nanoparticles covered an R6G concentration range of 4.5×10^{-7} M to 4.5×10^{-5} M. Initial curves showed a positive relationship between the concentration of analyte and the peak-area ratios defined previously. For the most recent curve, the citrate capped gold nanoparticles were placed in solution with 1-decanethiol via the multi-rinse method, and then equilibrated with the 2% V/V CS₂ prior to addition of R6G at concentrations of 4.0×10^{-6} M, 1.9×10^{-5} M, and 1.9×10^{-4} M R6G.

2.9 Reaction Monitoring Setup

A schematic for the reaction monitoring setup is depicted in Figure 2.7. Reactions take place in a quartz reaction vessel which is subjected to ultraviolet radiation from a UV lamp. The reaction remains on a constant stir in the reaction vessel, while a peristaltic pump is used to pump the reaction solution from an inflow tube through a cuvette at a constant flow rate, and then back to the vessel through an outflow tube. The cuvette has a window through which Raman spectra can be collected. For initial trials, the Raman system used

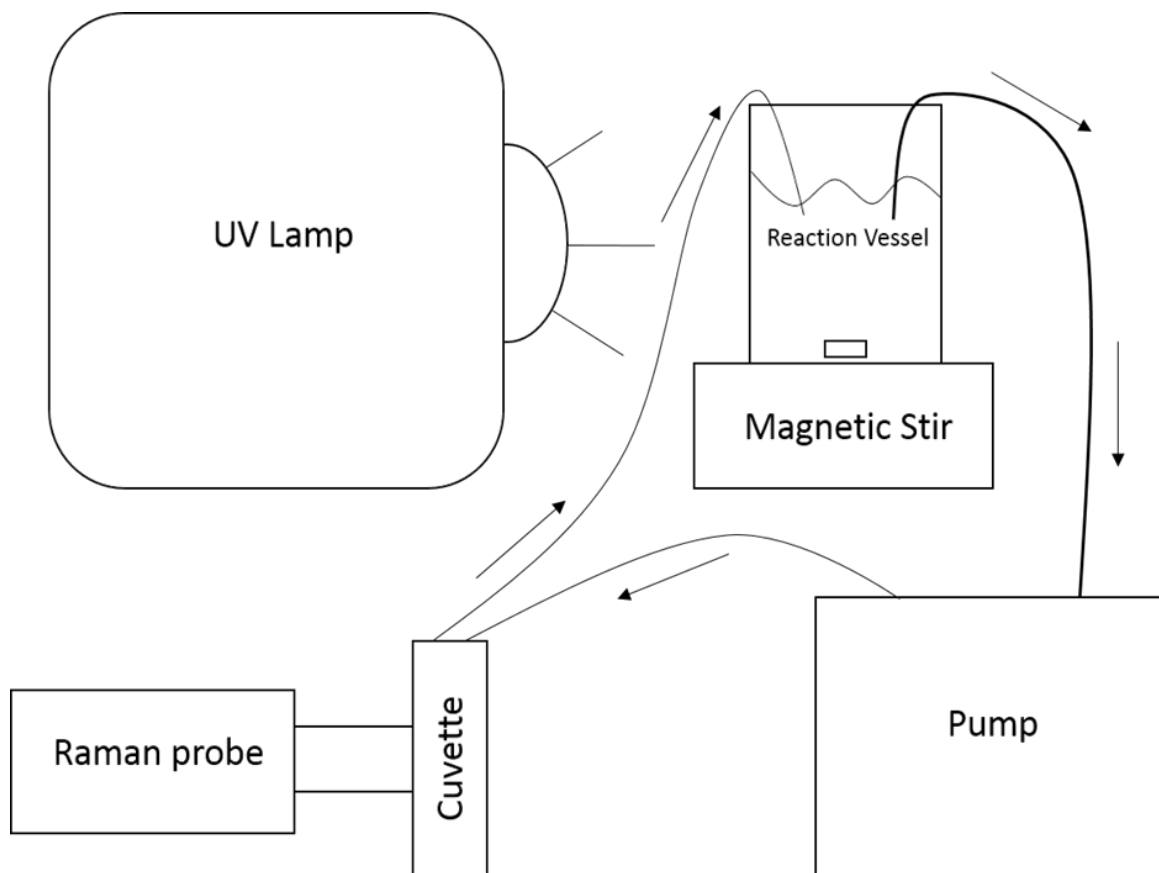


Figure 2.7: Reaction monitoring setup. The pumping setup for reaction monitoring. A suspension containing nanoparticles, analyte, and internal standard is placed on a constant stir in the quartz reaction vessel. Dependent on the trial, the reaction vessel may also contain TiO_2 , and the UV lamp may be on or off. The suspension in the reaction vessel is pumped via a peristaltic pump into a pumping cuvette with a solution window for data acquisition. The Raman system acquires Raman spectra at a rate of once every 11 s. In order to eliminate background noise to take reliable spectra, the Raman system and cuvette are kept in a dark environment to shield the detector from ambient light.

an integration time of 10 s, with a 1-s delay between measurements, such that spectra were generated once every 11 s.

CHAPTER 3

Results/Discussion: Addressing the Limitations of Raman Spectroscopy

The main categories of experimental data included in the Results/Discussion chapter are nanoparticle characterization, acquisition and analysis of surface-enhanced Raman spectra, calibration curve generation, improvement of nanoparticle stability, and reaction monitoring.

3.1 UV/VIS and TEM of Nanoparticles

The colloidal nanoparticle suspensions were characterized according to several important properties as described in Section 2.5. A rough estimate of nanoparticle size can be obtained by noting the optical properties of the colloidal suspension. Gold nanoparticles synthesized by a standard citrate reduction method have an amber-red color, depicted in Figure 3.1. As discussed previously, optical properties of colloidal gold nanoparticles are due to the property of surface plasmon absorption, which can be more quantitatively assessed using spectrophotometry in the ultraviolet and visible region (UV/VIS spectrophotometry). Figure 3.2(a) is an example of a UV/VIS spectrum of a sample of gold nanoparticles. The wavelength at which maximum absorbance occurs is assessed to determine the presence of surface plasmon resonance. The gold nanoparticles were determined to exhibit surface plasmon resonance at around 530 nm, which is consistent with that expected from the literature.⁴⁹ The wavelength at which surface plasmon

a)



b)



Figure 3.1: Image of gold nanoparticles. Appearance of colloidal gold nanoparticles a) newly synthesized nanoparticles in a round-bottomed flask b) sample of nanoparticles being stirred. The red color is consistent with nanoparticles roughly 30 nm in diameter.

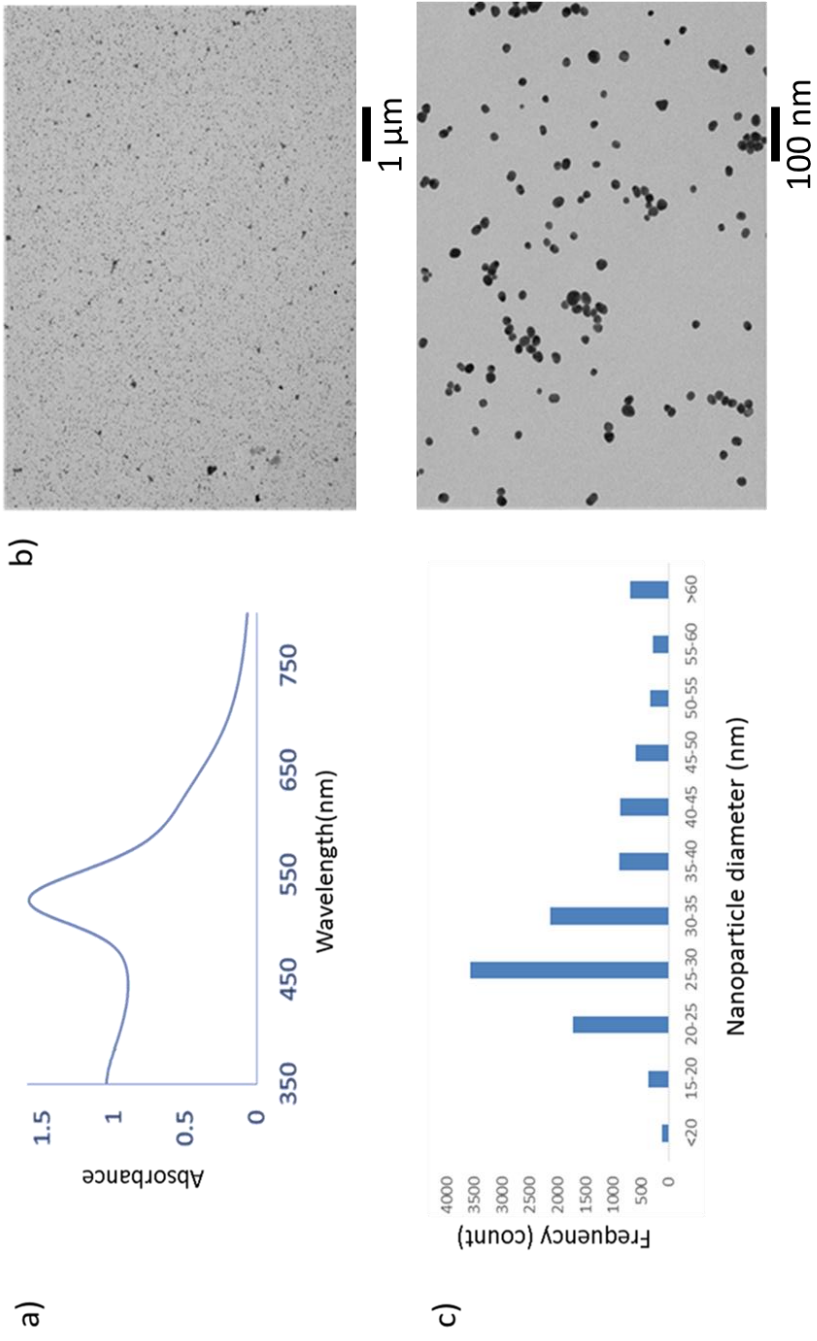


Figure 3.2: Nanoparticle characterization. a) UV/Visible spectrum of a 2-mL sample of 1:2 (colloid: deionized water) dilution of colloidal nanoparticles in aqueous solution taken by a UV/VIS spectrophotometer. The peak of the curve shown represents the maximum absorbance of the colloidal suspension, at 530 nm. b) Images taken using a transmission electron microscope (TEM) of a dried and treated sample of colloidal gold nanoparticles at 2000x (top) and 25000x (bottom) magnification. c) Frequency distribution chart indicative of the relative abundance of nanoparticles within the sample. Most of the nanoparticles lie within a range of 20-35 nm in diameter.

resonance occurs is important for our purposes because it must be near the wavelength of the photons emitted by the laser from in the Raman system (785 nm) but it should overlap with this wavelength, since overlap would interfere with signal due to significant fluorescence of the nanoparticles.

In order to obtain a better understanding of the distribution of size and shape in these nanoparticle suspensions, samples were analyzed using transmission electron microscopy (TEM). Figure 3.2(b) shows images of the dried nanoparticles at two separate magnifications, and it can be seen that they are roughly spherical, as anticipated. Additionally, these images were analyzed to generate a frequency distribution chart, shown in Figure 3.2(c), which shows the count of nanoparticles that have a diameter which falls within a particular range. The average diameter of the nanoparticles is 30 ± 20 nm, where the uncertainty is σ . It is notable that the nanoparticles are not necessarily uniform in size. Although precision is often desired in nanotechnology projects, it is very difficult to obtain, involving meticulous monitoring of temperature, time, stirring, and other factors during synthesis and storage. For the purposes of surface enhanced Raman spectroscopy, tight monitoring of uniformity in nanoparticle suspensions does not seem to be as important, and thus distribution of nanoparticle diameters is not a concern.

3.2 Increasing Sensitivity via Surface-Enhanced Raman Spectroscopy

Prior to collecting spectral data of analyte adsorbed onto gold nanoparticles, it is important to assess the appearance of spectra taken in the absence of analyte. A Raman spectrum of colloidal gold nanoparticles alone is shown in Figure 3.3, which is identical to what is observed in samples containing water, and spectra taken of the cuvette alone. Therefore, it was determined that the nanoparticles themselves do not contribute to the

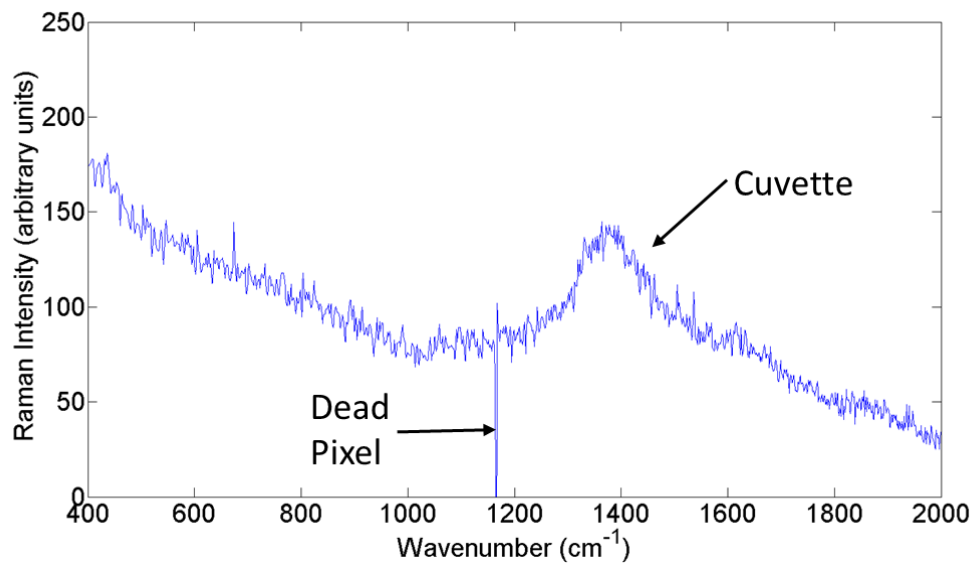


Figure 3.3: Raman spectrum of colloid alone. Particular spectral features, including the stretch associated with the cuvette and a dead pixel are labeled in the figure. Although the cuvette stretch is not visible in most spectra, it can interfere with spectra taken of particularly low analyte concentrations.

peaks seen in later spectra, they simply enhance the signal associated with adsorbed analyte. It is notable, however, that the cuvette does produce a broad bump-like stretch spanning from 1300cm^{-1} - 1500cm^{-1} which does not interfere with most spectra, but may sometimes be visible at low analyte concentrations at which signal intensity is somewhat weak. Additional controls were taken containing each analyte in aqueous solution without colloidal nanoparticles, and no analyte discussed in subsequent sections is able to be detected without surface enhancement, with the exception of the nitrate ion, which is discussed briefly in some contexts. These spectra appear identical to the control spectra shown in Figure 3.3.

To illustrate the effectiveness of SERS, Figure 3.4 depicts the difference between spectra of R6G in the absence and presence of gold nanoparticles. It is clear that signal is greatly enhanced by adsorption of analyte to nanoparticles, such that useful information can be deduced. Additionally, a powder spectrum of R6G was measured, as depicted in Figure 3.4(c), to ensure that signal is not significantly distorted by adsorption to nanoparticles in an aqueous environment. This is typically done for each analyte of interest. Although spectra in the aqueous phase can sometimes be altered due to the effects of solvation from water and ionic strength on molecular vibrations, variation usually manifests as a slight shift of spectral peaks, or a change in the relative intensities of peaks, which does not impede the ability to provide a cursory justification of effective SERS signal. It should, however, be considered in later computational analysis. Additionally, it does not seem that spectra are significantly altered due to adsorption of the analyte onto nanoparticles, beyond what could reasonably be expected from solvation and ionic strength effects from dissolving the analytes in aqueous solution. This is important for reaction

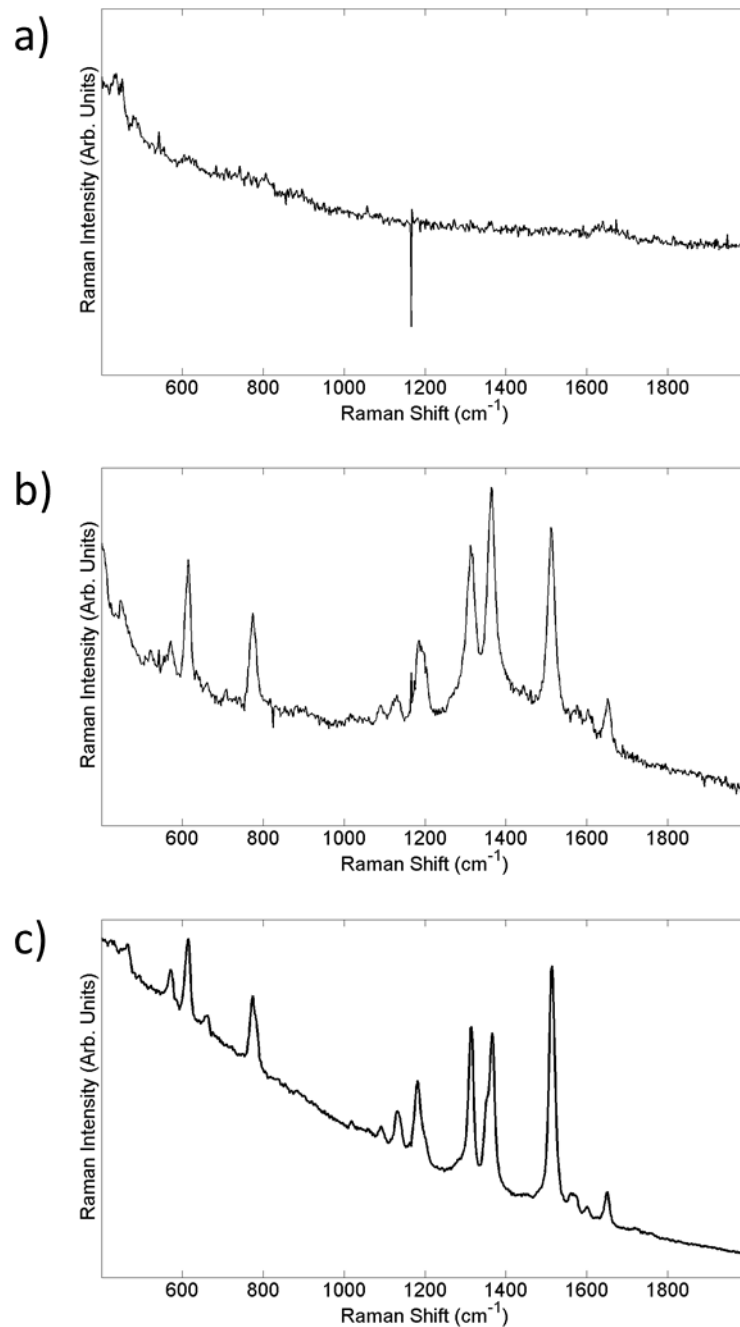


Figure 3.4: R6G SERS. To demonstrate the use of surface enhanced Raman spectroscopy, it is shown that for a 10^{-7} M solution of R6G: a) in the absence of gold nanoparticles no useful signal is observed, b) in the presence of nanoparticles signal is greatly enhanced, exhibiting nearly all spectral peaks expected, with differences in the intensity pattern, c) a powder Raman spectrum for comparison to surface enhanced spectra.

monitoring via analysis of spectral features, because it suggests that the presence of nanoparticles does not significantly alter vibrational modes, it only serves to expand detection limits via surface enhancement.

Surface-enhanced Raman spectra have also been measured for the ionic pesticide paraquat, as depicted in Figure 3.5(a). Aside from its direct relevance to wastewater treatment (discussed in the introduction), paraquat is of particular importance due to computational efforts that have been made by John Bertram, another student working in the Nee lab. The calculated Raman spectrum aligns closely with the powder Raman spectrum, as depicted in Figure 3.5(b). Additionally, it can be seen in Figure 3.5 that the surface-enhanced Raman spectrum of paraquat dissolved in aqueous solution with nanoparticles is also aligned with both computational and powder data. Since the computational data includes a summary of the vibrational modes associated with each spectral peak, alignment allows confident predictions regarding the structure of intermediate species arising over the course of a reaction. For example, the circled peaks in Figure 3.5(a) and Figure 3.5(b) at 1350 cm^{-1} are indicative of an inter-ring stretch, which is illustrated in Figure 3.6. A change to the peak at 1350 cm^{-1} over the course of a reaction could indicate a break separating the two rings, additions at involved atoms, or any other changes that could alter the ability of the molecule to make this vibration, or the energy associated with it. Similar procedures can be done for all observed peaks, however some of these peaks correspond to more delocalized vibrational modes, which are less useful for deducing specific functional group alterations from spectral features alone.

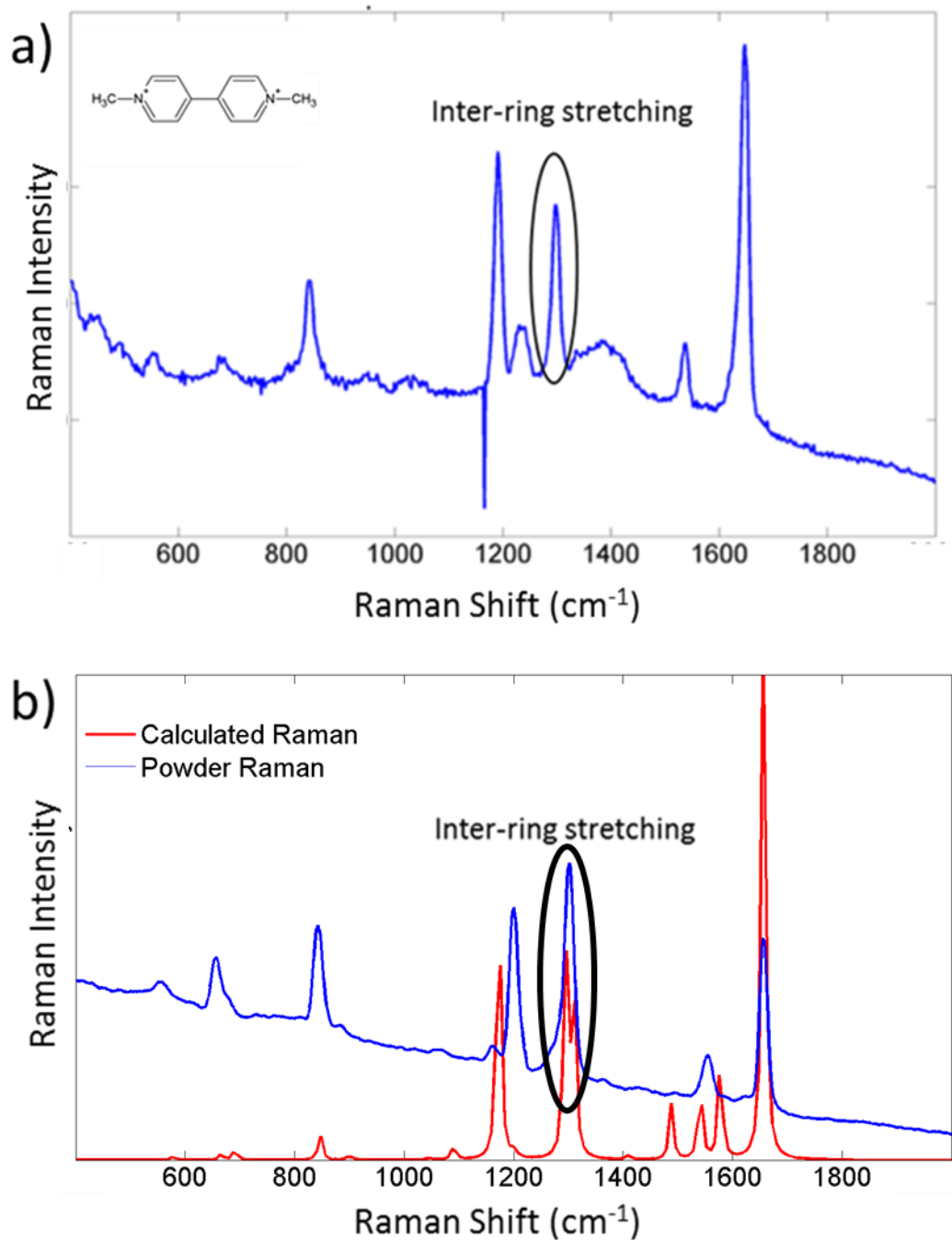


Figure 3.5: Computational and SERS paraquat data. An example of the relationship between spectral information and changes in analyte over the course of a reaction. a) A surface-enhanced Raman spectrum of 2×10^{-5} -M paraquat solution compared to b) computational data (red) which closely aligns with a powder spectrum of paraquat (blue). A particular peak in each figure is marked with an oval, corresponding to a vibrational mode of the paraquat molecule illustrated on the following page.

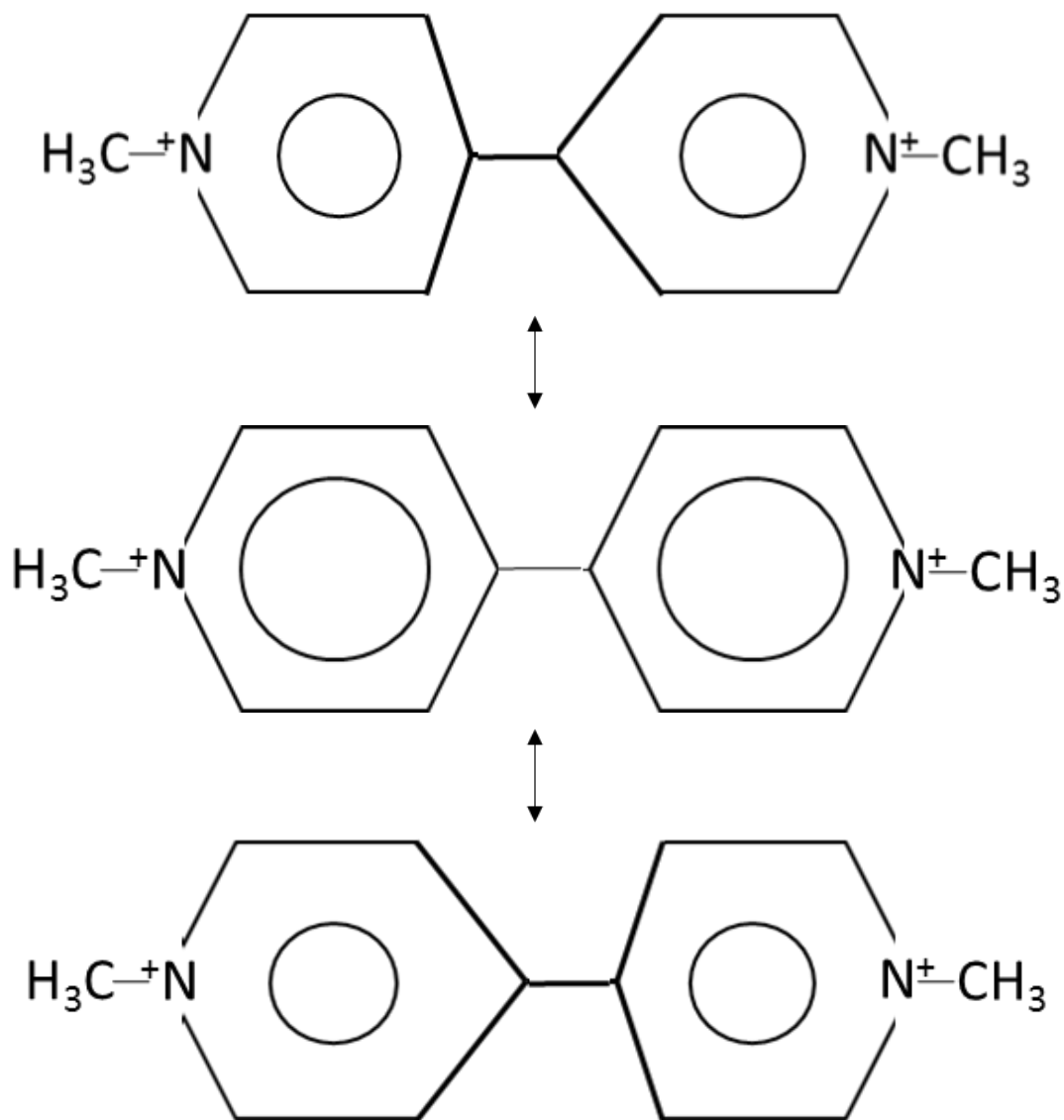


Figure 3.6: Paraquat stretch. Labeled inter-ring stretching of paraquat. In the middle, the structure of paraquat is shown in a standard form. The images on the top and bottom represent the conformations of paraquat during this particular molecular vibration, during which the carbon atoms bonded to one another in each aromatic ring shift to the left or right relative to the symmetrical axis of the molecule, without a change in the length of the bond between them. This vibration occurs when the molecule is subjected to a specific amount of energy, corresponding to photons of at the wavenumber depicted in Figure 3.5.

3.3 Calibration Curves for Quantitative Purposes

To quantitatively assess the kinetics of reactions via *in-situ* monitoring, calibration curves were generated. These curves allow the intensity of spectral features to provide information regarding analyte concentration. Tracking changes in analyte concentration over the course of the reaction is essential to understanding the reaction rate. Concentration can be assessed via the introduction of an internal standard (CS₂) as a point of reference, as discussed in Section 2.8. Figure 3.7 shows the spectral differences between SERS spectra of R6G alone, CS₂ alone, and the two coupled together. Coupling of analyte and internal standard has also been done for paraquat, which exhibits less overlap with the internal standard than does R6G, as shown in Figure 3.8.

Although specific values for Raman intensity vary from spectrum to spectrum due to instrumental variabilities associated with Raman spectroscopy, the introduction of a constant concentration of internal standard can provide a point of reference for use in a ratiometric approach to determining analyte concentration. This idea is best illustrated qualitatively by considering a few data points which were used in the generation of a calibration curve. Figure 3.9 depicts spectra of suspensions containing identical concentrations of CS₂, and R6G concentrations of 5×10^{-7} M, 5×10^{-6} M, and 5×10^{-5} M. When the concentration of R6G is increased there is no change in the intensities of peaks from R6G relative to one another. However, in comparison to the single peak of CS₂, peaks from R6G are relatively more intense as the concentration of R6G is increased. Therefore, although the specific values for the intensity of R6G cannot be correlated to its concentration, the relationship between the peaks of R6G and the peak of an internal

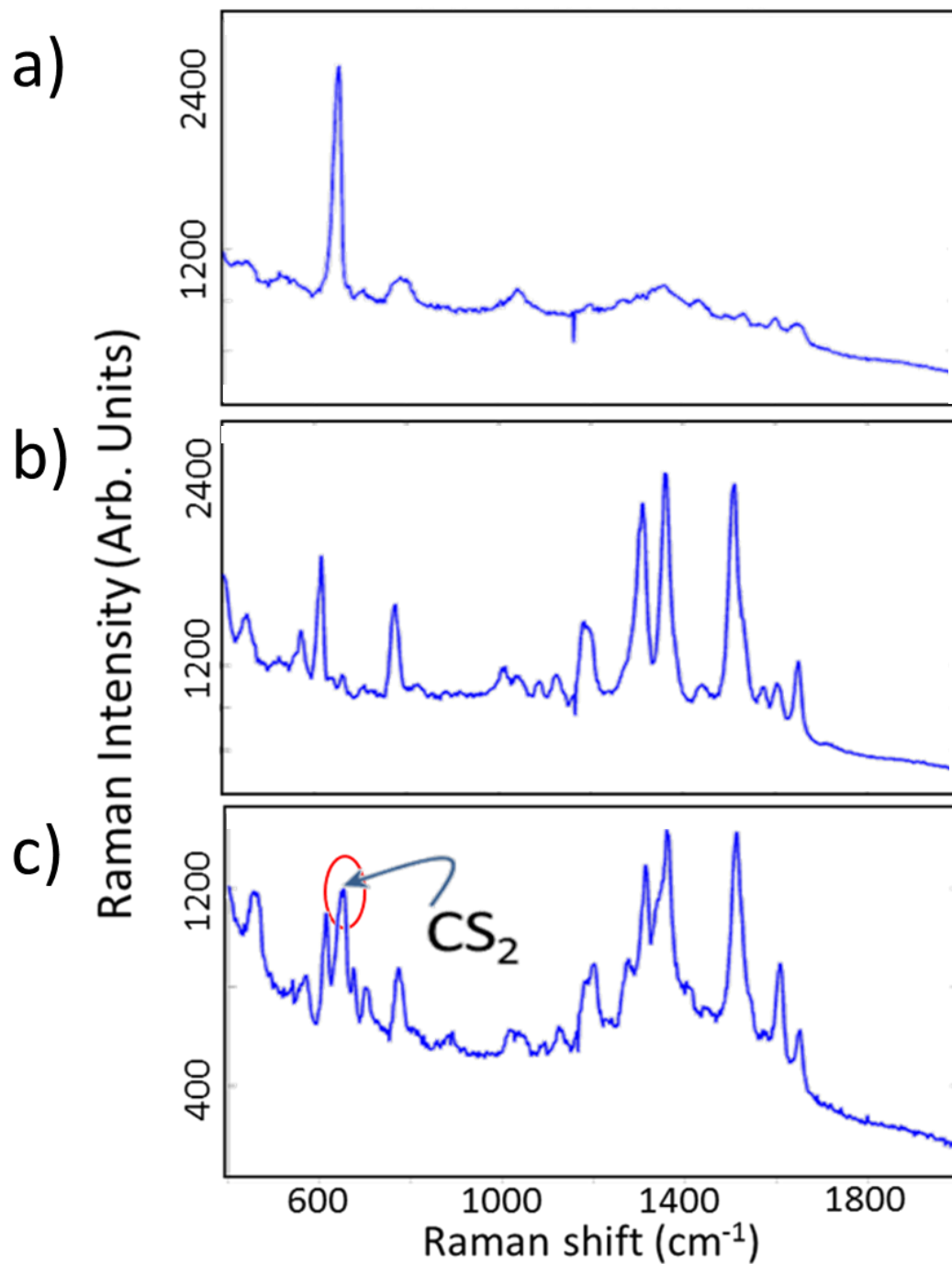


Figure 3.7: R6G coupled to internal standard. Coupling of internal standard carbon disulfide (CS₂) to Rhodamine 6G (R6G). a) CS₂ SERS alone shows a single peak; b) R6G SERS alone, c) R6G coupled with internal standard, peak from internal standard is labeled with a red oval.

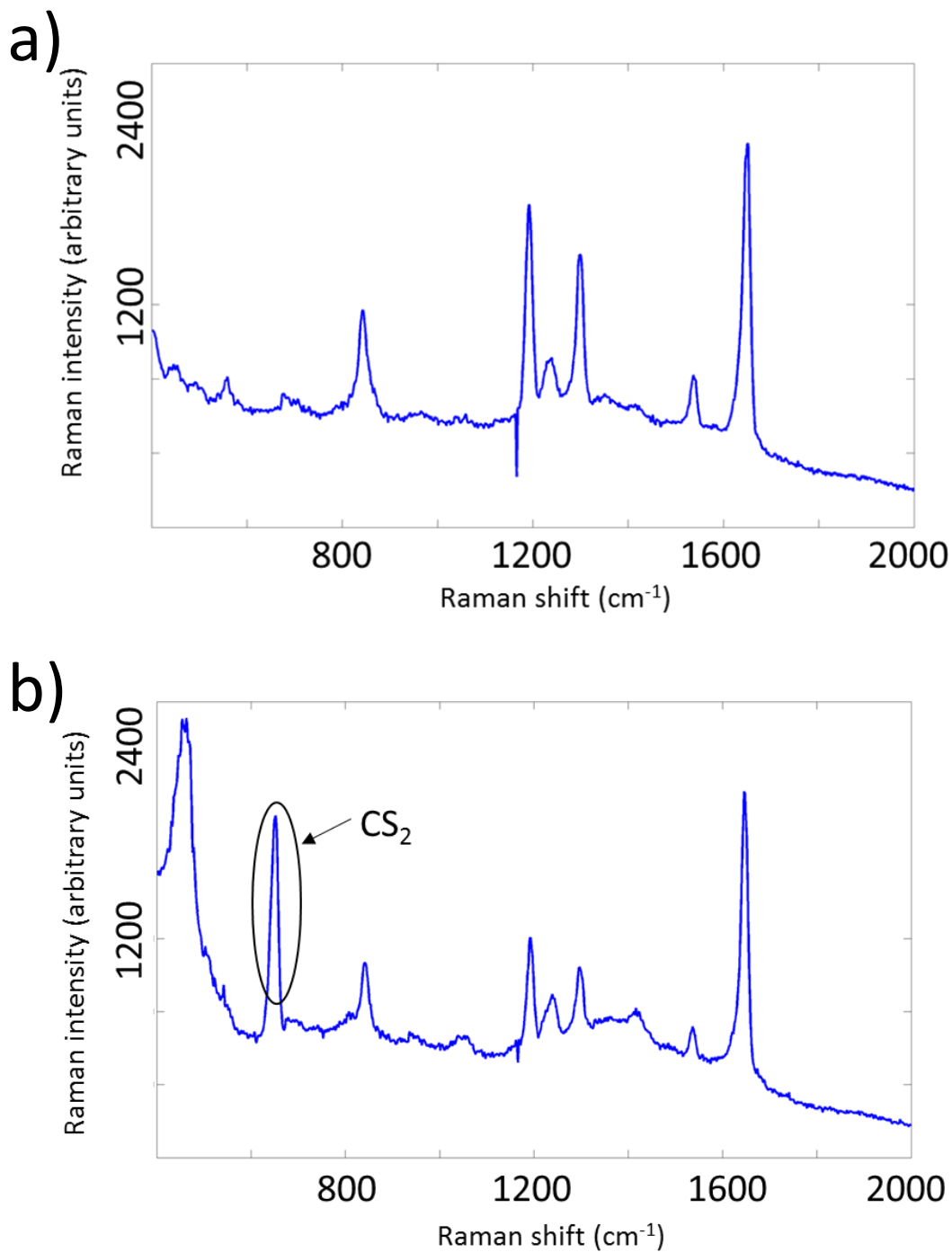


Figure 3.8: Paraquat coupled to internal standard. Coupling of internal standard to paraquat. a) SERS spectrum of paraquat alone; b) SERS spectrum of paraquat coupled with carbon disulfide. The single peak of CS_2 is labeled in black, which exhibits less overlap than R6G. This demonstrates the ability to expand to compounds more relevant to wastewater treatment than R6G.

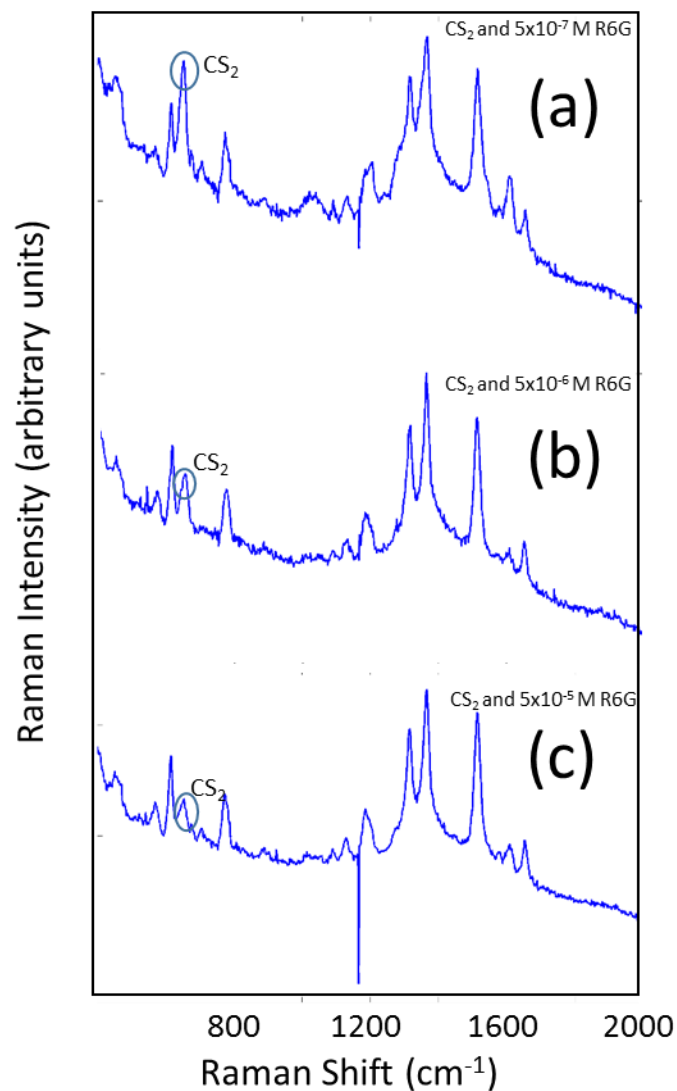


Figure 3.9: Ratiometric approach R6G. Coupled spectra of R6G and CS₂ as the concentration of R6G increases from top to bottom. a) 5x10⁻⁷-M R6G solution; b) 5x10⁻⁶-M R6G solution; c) 5x10⁻⁵-M R6G solution. The CS₂ peaks appear to diminish even though its concentration is the same throughout, because the peaks of R6G become more intense relative to CS₂ as its relative concentration increases.

standard can be correlated to R6G concentration, as long as the concentration of CS₂ is constant.

Two preliminary calibration curves for the test analyte, R6G, are depicted in Figure 3.10. These are plots of the ratio of integrated areas of Gaussian curves fit to spectral peaks of the analyte (608 cm⁻¹, 1509 cm⁻¹, and 1360 cm⁻¹) relative to that of the peak from the internal standard (650 cm⁻¹), versus the concentration of analyte. From this, if a constant concentration of internal standard is in a monitored solution, it is possible to determine the change in analyte concentration over the course of the reaction by calculating the ratio between analyte peaks and the internal standard peak. The most important thing to note from the preliminary plots is that although the precise relationship between intensity ratios and concentration is unclear, ratios for spectral peaks relative to internal standard peaks increase as analyte concentration increases, whereas the ratio of any two peaks in a given analyte remain constant over the concentration range. This is crucial, because it implies that a ratiometric approach is more suitable for our purposes than directly monitoring changes in peak intensity or peak area, which do not correlate as well with concentration. Further development of these calibration curves (discussed in Section 3.6) has required more effort in nanoparticle aggregation and stabilization. Nanoparticle stabilization efforts were inspired by initial reaction monitoring trials, which had proven to be unsuccessful due to over-aggregation of nanoparticles.

3.4 Initial Reaction Monitoring

Once the internal standard had been introduced, and preliminary calibration curves were generated, the project moved forward into an initial reaction monitoring trial. The setup discussed in Section 2.9 was tested to ensure that it could effectively maintain

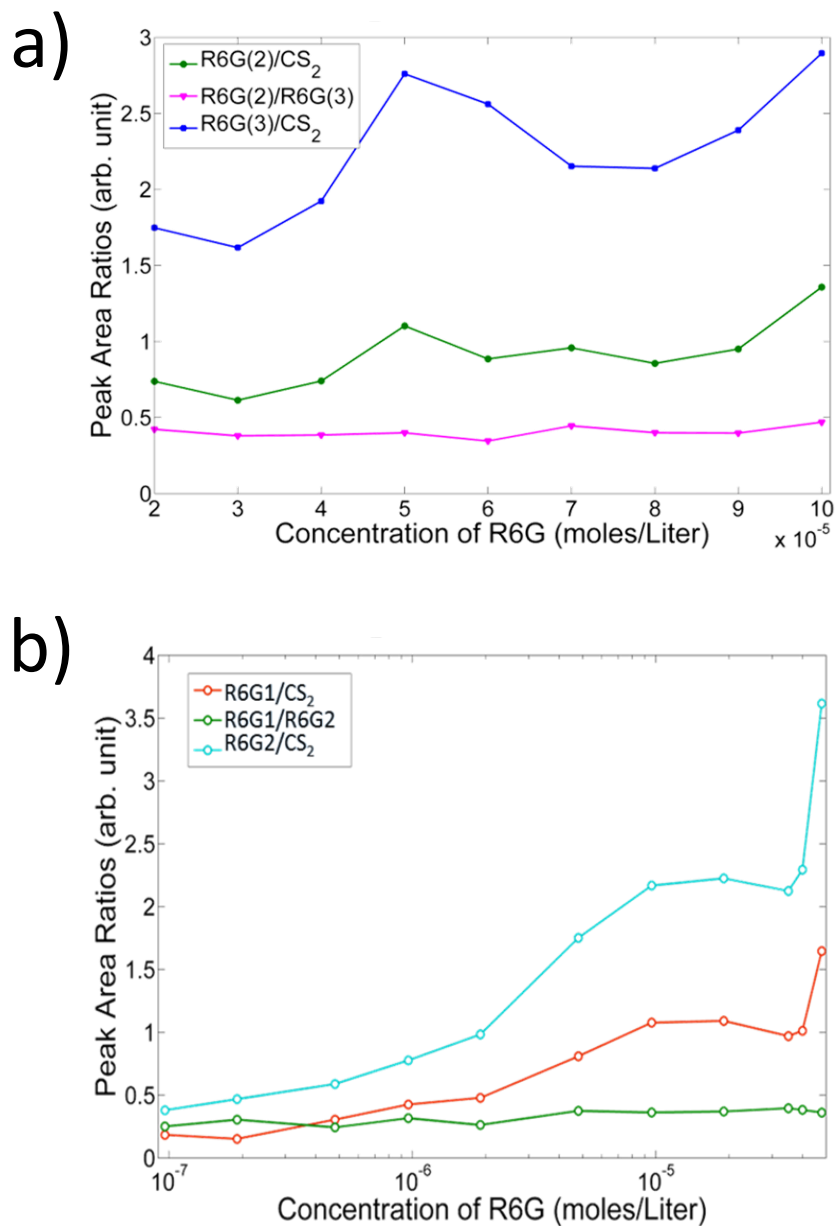


Figure 3.10: Preliminary R6G calibration curves. Two preliminary calibration curves demonstrating the potential for use of CS₂ as an internal standard. Note that the scale is different in each: a) the first plot generated uses a standard scale, whereas b) the second curve generated uses a logarithmic scale on the x-axis to linearize this data set since it covers a wider range of concentrations spanning three orders of magnitude. R6G1, R6G2, and R6G3 correspond to spectral features at 608 cm⁻¹, 1509 cm⁻¹, and 1360 cm⁻¹, respectively. The spectral feature corresponding to CS₂ is at 650 cm⁻¹.

accurate measurement over an extended period by pumping 25 mL of a 1-M potassium nitrate solution, and signal was somewhat less intense than what would be seen under normal conditions, but still visible. Again, R6G was chosen as an initial test species. Once visible signal was confirmed, the first control trial containing R6G, CS₂, and nanoparticles under constant stirring in the absence of TiO₂ and ultraviolet radiation was attempted. An example of the results of these initial attempts is represented by Figure 3.11, which plots selected peak area ratios as a function of time.

Initial reaction monitoring trials showed considerable variability which needed to be addressed. Signal diminished as a function of time once the nanoparticles were initially aggregated due to the constant stirring required by the reaction monitoring setup. Since work done up until this point had been concerned with immediate measurement rather than measurements over time, this factor had not been previously considered. Over-aggregation of nanoparticles causes clumping and subsequent decrease in signal, which makes nanoparticle stabilization important to monitoring reactions over time. Nanoparticle stabilization would also allow for the generation of more reliable calibration curves, eliminating variability caused by disparities in time of data acquisition for each measurement.

3.5 Nanoparticle Stability

Although nanoparticle aggregation is important for acquiring SERS spectra, we have found it to be effective only in the short-term. When the aggregated nanoparticles are subjected to a constant stir, crystal growth is even more heavily favored such that nanoparticle flocculation results. Most simply stated, flocculation is to a colloidal suspension as precipitation is to a solution. Here, it leads to formation of visible clumps

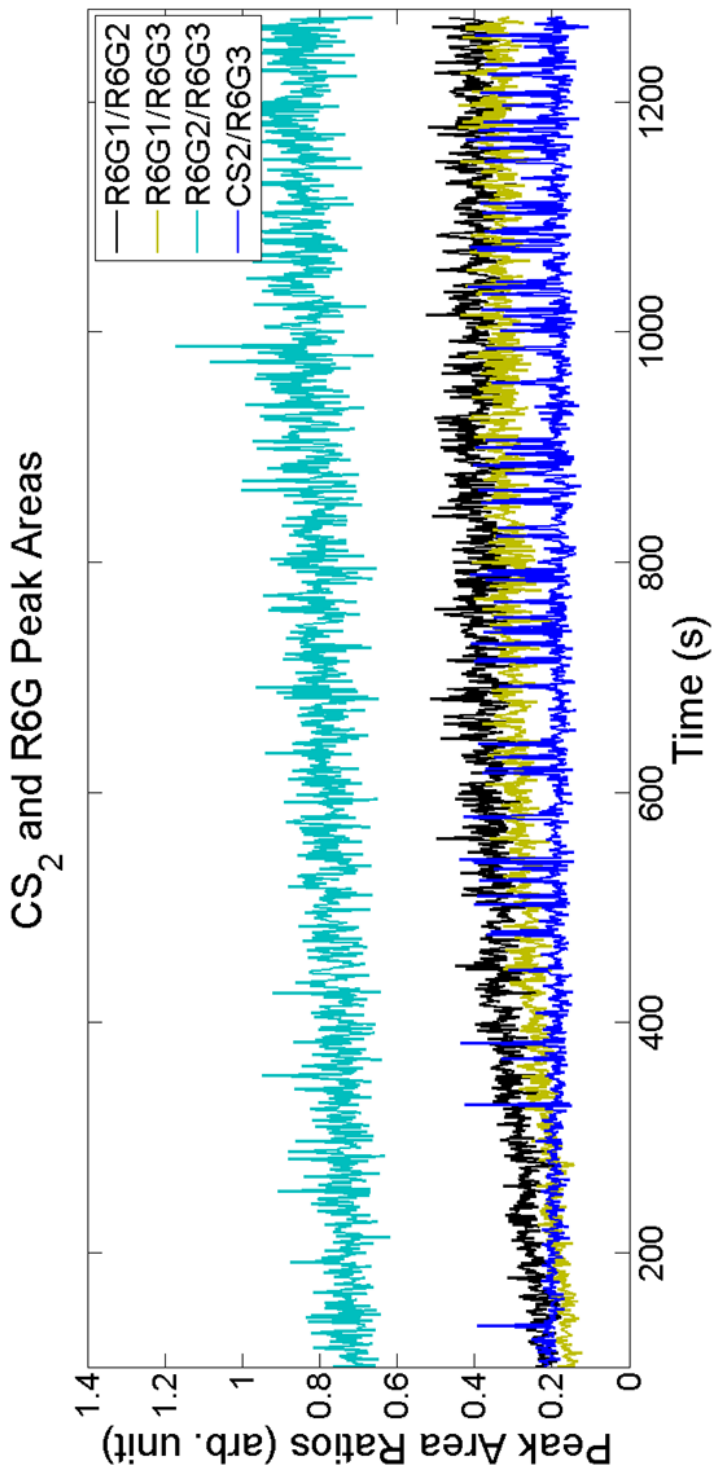


Figure 3.11: Photocatalytic degradation initial control trial. A plot of the ratios between some selected peaks of R6G and the peak of the CS₂ internal standard as a function of time in the absence of UV radiation or TiO₂. Over time, the nanoparticles lost stability, and considerable clumping lead to a loss of signal.

and SERS signal diminishes. When the nanoparticles are originally dispersed in a colloidal suspension due to electrostatic forces, a loosely packed secondary layer of charged ions surrounds them and prevents aggregation of the nanoparticle cores that would occur if they were brought into close proximity. Addition of electrolyte decreases the volume of the loosely packed secondary layer, and allows nanoparticle cores to come into sufficient proximity for aggregation.⁵⁸ Initially, this brings positively charged analyte into close association with colloidal nanoparticles, and thus promotes signal enhancement. However, subsequent stirring of the semi-aggregated suspension promotes flocculation to form large aggregates, which are no longer effective for surface enhancement.

The aggregation process and its effect on signal can best be illustrated using an example in which a Raman-active electrolyte is used as an aggregating agent, as shown in Figure 3.12. Experiments were conducted to determine the cause of signal diminishment resulting from stirring in our initial reaction monitoring trials. Figure 3.12(a) depicts a spectrum of 10^{-7} -M-paraquat and 0.2-M-sodium nitrate (aggregating agent) solution, along with a corresponding cartoon depiction of two nanoparticles in the suspension and the associated ions in their primary and secondary layers. Nitrate is not a SERS-enhanced substrate: the signal intensity of nitrate is the same as it would be in the absence of nanoparticles. Initially, aggregation places the analyte in “hot spots” between two nanoparticle cores, and greatly enhances signal. Figure 3.12(b) shows the spectrum and associated cartoon diagram of the suspension after 5 minutes of stirring. The nanoparticle cores come together, displacing paraquat from the SERS hot spot and simultaneously blocking signal via electrostatic interactions with the nitrate ion. The cartoon depictions were determined based on the change in spectral features caused by stirring. Since the

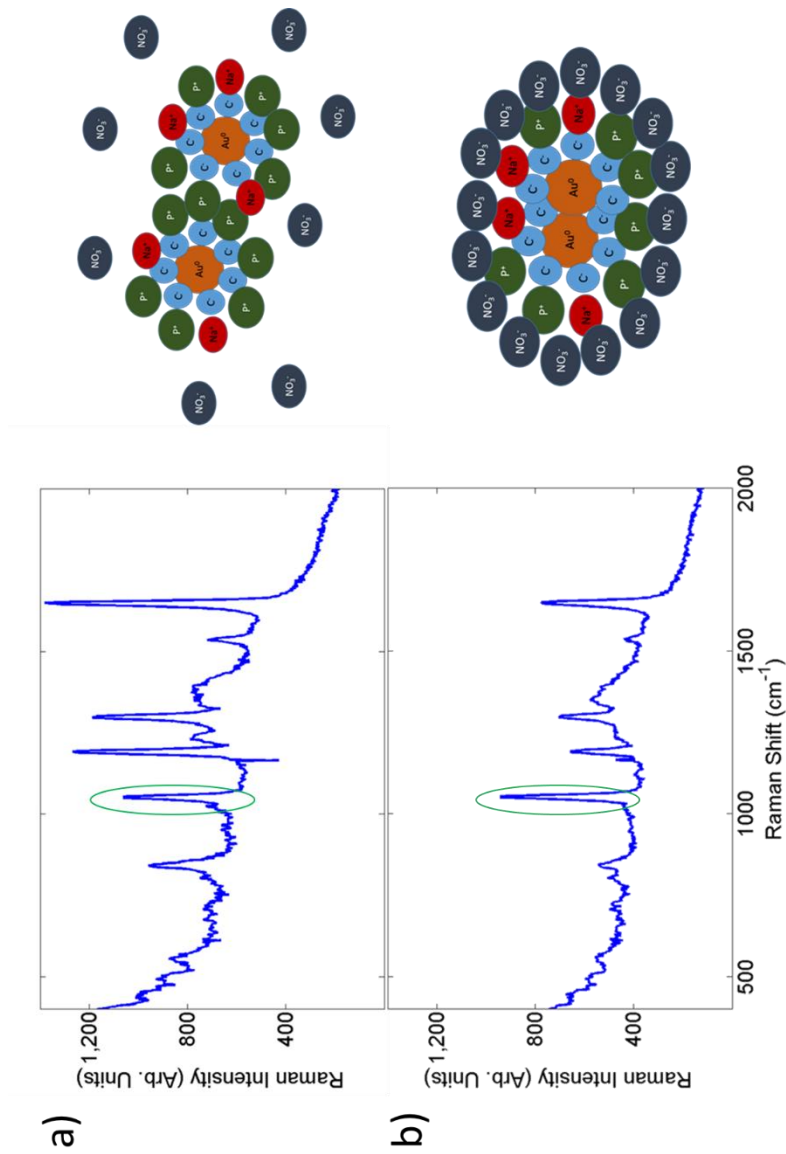


Figure 3.12: Aggregation demonstration using nitrate. The problem associated with nanoparticle aggregation in the context of reaction monitoring. a) initial conditions compared to b) conditions after a period of stirring lasting 5 min. Signal intensity associated with paraquat diminished, relative to that associated with the aggregating agent, nitrate ion. The stretch from nitrate (1050cm^{-1}) is labeled with a green oval, while all other observed stretches are associated with paraquat. In the cartoon diagrams, Au⁰ represents the nanoparticle core, C⁻ represents the citrate capping agent, Na⁺ represents sodium ions, P⁺ represents paraquat, and NO₃⁻ represents the nitrate ion.

paraquat stretches decreased relative to the nitrate stretch over time even though the relative concentrations of these species were unchanged, this implies some displacement of paraquat from a position favorable for surface enhancement, and potential signal blocking caused by the electrolyte itself. The dominant effect contributing to signal diminishment is most likely the displacement of the analyte from SERS hot spots.

As it became clear that citrate-capped nanoparticles experienced significant clumping and aggregation when subjected to the constant stirring required for the reaction monitoring setup, efforts began to focus on stabilizing the nanoparticles such that they could maintain reliable signal over a period of time long enough to gain useful information about photocatalytic reactions. One way to stabilize the nanoparticles is to partially displace citrate with mid-chained thiol compounds such as 1-decanethiol, as discussed in Section 2.7. The binding of thiolated compounds to the nanoparticle core provides a layer of steric stabilization which helps to prevent nanoparticle aggregation.⁶² For our purposes, it is important that citrate is only partially displaced, because full displacement of citrate by 1-decanethiol results in change of nanoparticle diameter from 25-35 nm to as small as 2-5 nm, which do not have appropriate optical properties to be useful as SERS substrates.

The concentration of 1-decanethiol needed for nanoparticle stabilization is not well established at this time. Since 1-decanethiol is almost entirely insoluble in aqueous solution, any measureable volume placed in 25-mL aliquots of nanoparticle colloid exceeds its solubility. Excess 1-decanethiol causes formation of smaller nanoparticles, and thusly initial attempts to stabilize nanoparticles resulted in nanoparticles which were ineffective for SERS. In contrast, the current procedure for the implementation of 1-decanethiol to the colloidal gold nanoparticles involves the rinsing process described earlier. The uncertainty

regarding the true concentration of 1-decanethiol in sample sets presents a potential obstacle to be faced for analysis of larger sample volumes, but the results that follow provide a conceptual verification that 1-decanethiol in minute concentrations is effective at increasing the stability of nanoparticles used for SERS.

The nanoparticles synthesized in lab require some initial aggregation in order to reach optical properties which are optimal for use in SERS. Analytes which exhibit the strongest SERS signals are generally cationic species present as salts, such as R6G and paraquat. Analytes which are not present as electrolytes require the simultaneous addition of a Raman-inactive electrolyte such as sodium chloride to the nanoparticles in order to exhibit SERS signal. It is therefore clear that in the short-term, nanoparticle aggregation is important for SERS. However, when semi-aggregated nanoparticles are subjected to a constant stir, the rate of aggregation increases and nanoparticles quickly lose optical properties appropriate for SERS. Figure 3.13 provides a comparison between the UV/VIS spectrum of un-aggregated and semi-aggregated nanoparticles. The shift is also visible to the eye, as the solution colloid changes from red to dark purple upon aggregation, and gradually becomes colorless as aggregates precipitate out of solution.

Perhaps the most important quality of 1-decanethiol capped nanoparticles is their ability to become semi-aggregated without quickly proceeding to a point which is no longer effective for data acquisition. If 1-decanethiol is added immediately before the addition of the analyte, (along with an aggregating agent, if necessary) then the nanoparticles will quickly undergo initial aggregation, but the process is halted during a point at which the nanoparticle aggregates are an appropriate size for SERS. Figure 3.14 illustrates the effectiveness of this for a particular analyte, R6G. 1-decanethiol was introduced to the

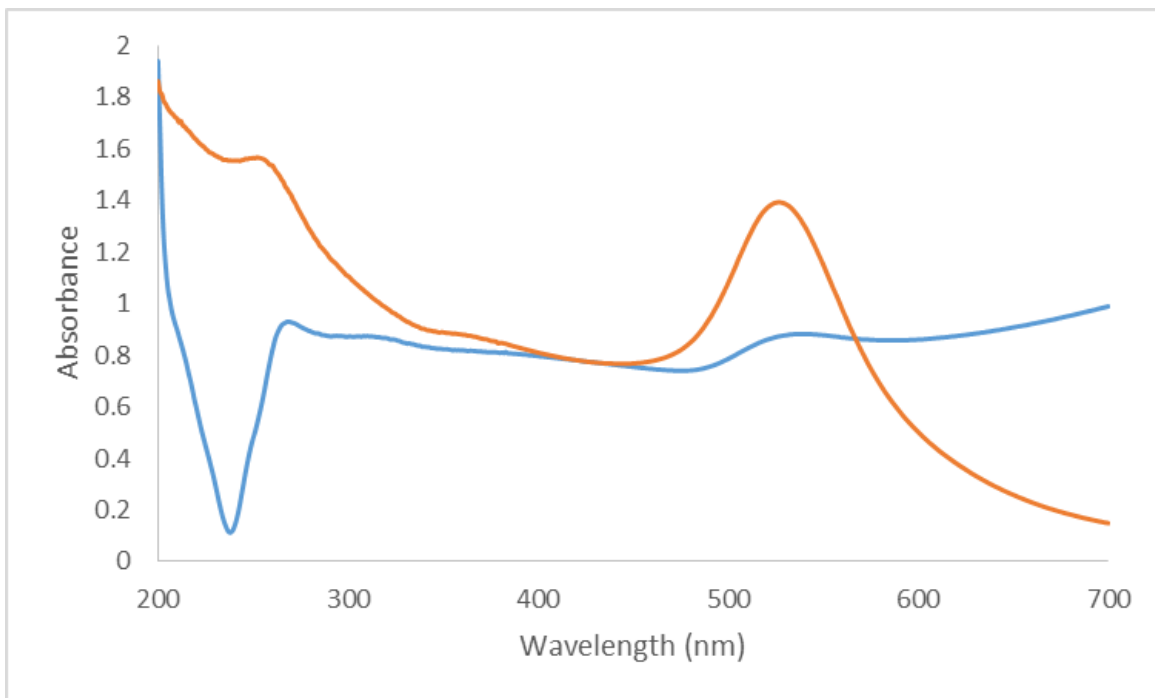


Figure 3.13: UV/VIS aggregated/un-aggregated comparison. UV/VIS spectra of gold nanoparticles. The orange curve is from a diluted solution of colloid alone, while the blue curve is from colloid aggregated with 40 microliters of 0.1M NaCl.

nanoparticle solution via the multi-rinse method, and equilibrated with a five minute stir prior to addition of R6G. A Raman spectrum was taken immediately, and then again after 1 hr under vigorous stir. Without introduction of 1-decanethiol as a secondary capping agent, nanoparticles aggregate within 5 min of moderate stirring such that signal is almost entirely lost. By contrast, Figure 3.14 shows that there was no loss in Raman signal over a full 1-hr period with secondarily-capped nanoparticles. This is crucial, because it shows that not only are nanoparticles stabilized from aggregation over much longer lengths of time due to secondary capping, but also that this effect does not compromise the Raman spectrum of the analyte over time.

3.6 Calibration Curves with Secondarily-Capped Nanoparticles

The secondary capping of nanoparticles in order to increase nanoparticle stability is essential for monitoring reactions over an extended time period. It should also, in theory, be beneficial for the generation of calibration curves. One of the sources for error in the calibration curves discussed earlier is that nanoparticle aggregation was not controlled, and therefore the time of data acquisition introduces a new variable which caused deviation from anticipated trends. With the stabilization of nanoparticles at a constant size and relative abundance of bound analyte, deviations due to time are no longer a factor.

Initial calibration curves generated using the secondarily capped nanoparticles are promising. Although at the time of this writing insufficient trials have been performed to obtain a standard, reliable calibration curve, Figure 3.15(a) shows a preliminary calibration curve which includes three data points, each representing a concentration of R6G at a different order of magnitude. A more qualitative sense of the data points is depicted in Figure 3.15(b), in which the peak of the internal standard is labeled and the remaining

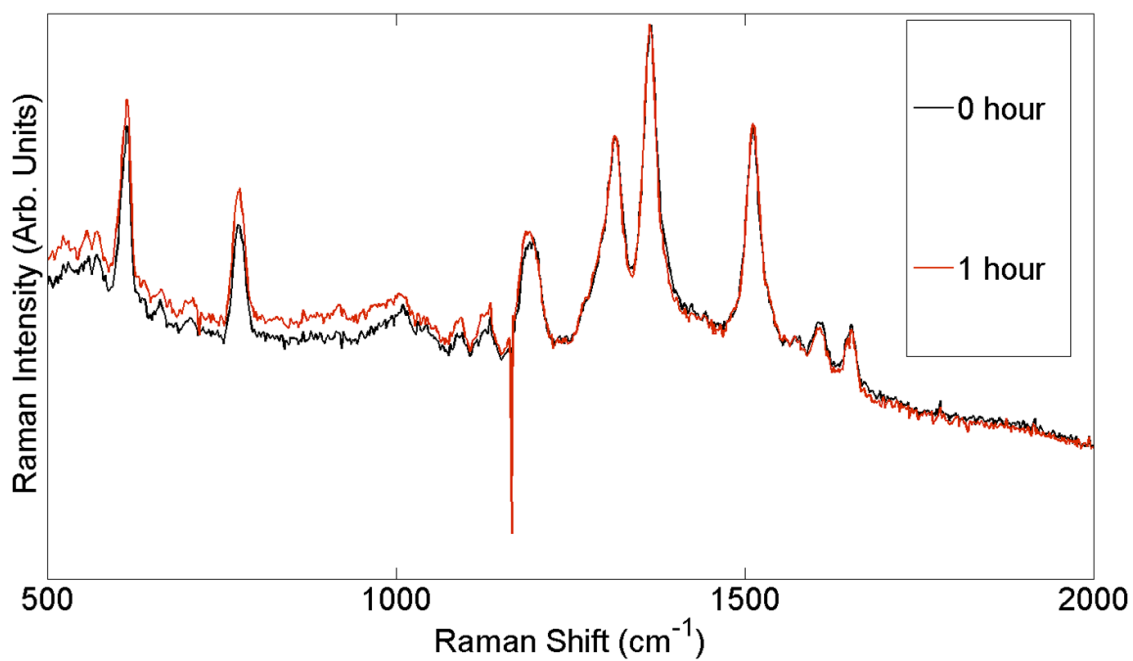


Figure 3.14: Nanoparticle stability demonstration. SERS spectra of R6G using 1-decanethiol secondarily capped gold nanoparticles. The mid-chained thiol displacing some citrate molecules acts to sterically stabilize semi-aggregated gold nanoparticles such that signal intensity is maintained. As shown, signal intensity does not diminish from (black) immediately after the introduction of R6G to (red) one hour of constant stirring later. Without secondary capping to stabilize the semi-aggregated nanoparticles, no signal is observed after an hour of stirring.

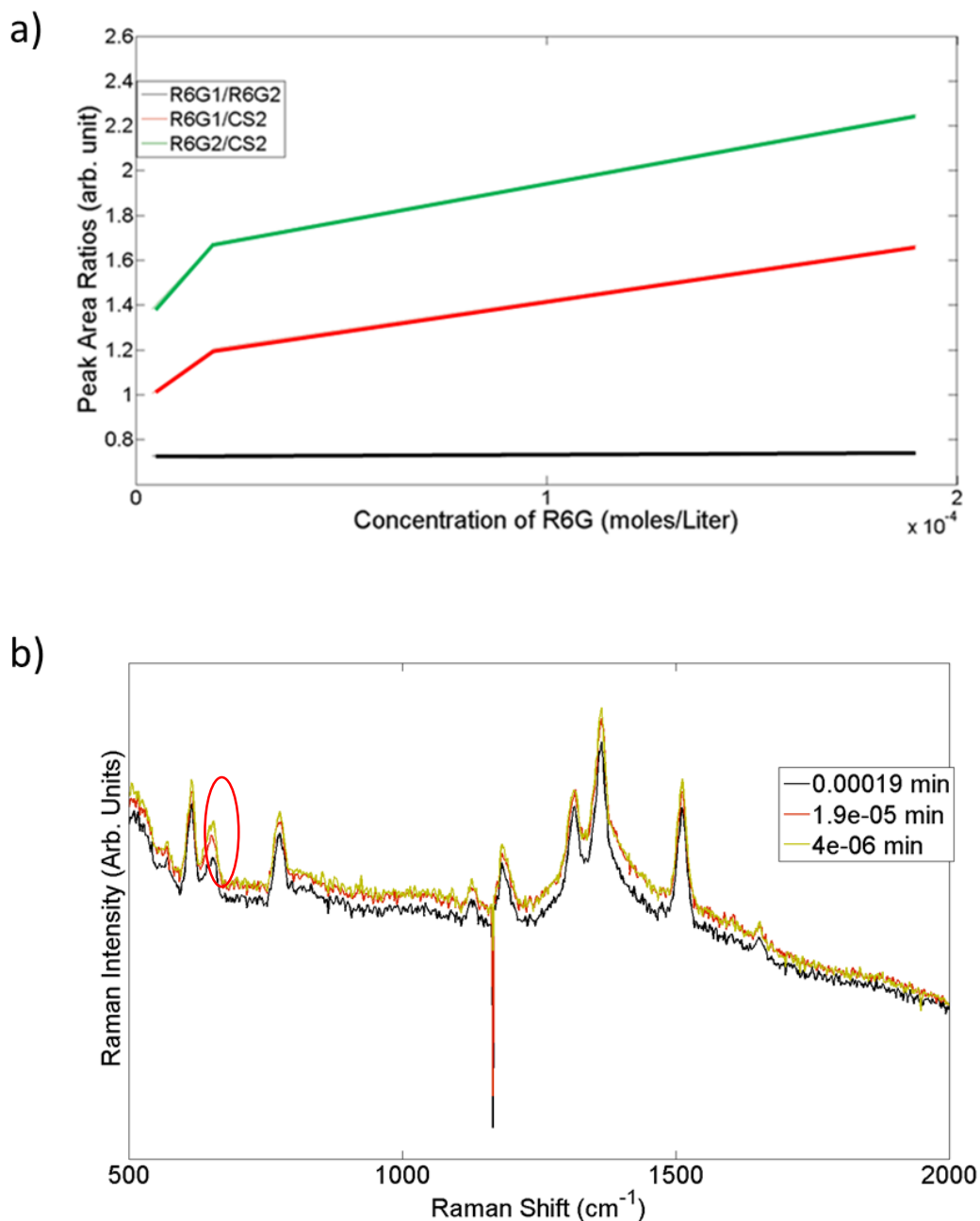


Figure 3.15: New calibration curve. Calibration curve for R6G using 1-decanethiol secondarily capped citrate gold nanoparticles. a) Depicts the three-point calibration, over a concentration range of 4×10^{-6} M to 1.9×10^{-4} M R6G. The relationship appears to be roughly linear over this range, however more intermediate data points will be collected in subsequent trials, with the general limits to the range now established. b) Overlapping spectra of each concentration of R6G coupled with the internal standard. The peak of the internal standard is marked with a red oval.

peaks are from R6G. Although more data points were collected than those included in the calibration curve, those below 4×10^{-6} M R6G did not exhibit enough spectral signal to be useful, and those above 1.9×10^{-4} M R6G were saturated and thus did not increase in peak area due to increase in concentration. Therefore, the reported range is currently the limited range of detection for our secondarily-capped nanoparticles. This range may be expanded to lower R6G concentrations by introducing additional electrolyte concurrently with R6G in order to more effectively induce aggregation at low concentrations of analyte. In future studies, more intermediate data points should be collected to clarify the trend over this range, and data points will be collected in triplicate to allow for error determination associated with reported values. In a practical sense, a three-point calibration such as this one may be sufficient for each individually prepared thiol-capped colloid prior to monitoring reactions, especially if the relationship can be shown to be linear over this limited range of concentrations. It is likely that each time a newly prepared colloid is used for monitoring reactions, an aliquot will need to be used to generate a working calibration curve, since each colloid has a slightly different size distribution, and the concentration of 1-decanethiol is not presently well-controlled. This is mentioned to emphasize the point that a single, universal calibration curve for a particular compound at a particular concentration of internal standard is unlikely to be achievable due to the degree of variability possible in the various aspects of the experimental preparation. The only way to account for this is to generate a new calibration curve in the same manner for each individual solution which is to be monitored. However, once the calibration is performed, the entire reaction time can use one calibration.

The range of concentration depicted in the discussed calibration curve is the range over which quantitative reaction analysis will be effective using these thiol-capped semi-aggregated gold nanoparticles. Concentrations of R6G lower than 10^{-6} M are difficult to visualize with SERS when coupled with the internal standard CS₂. Spectra of such low concentrations are distorted. Concentrations of R6G much higher than 10^{-4} M quench signal such that peak intensity does not increase with addition of more analyte. Thus, for the secondarily capped nanoparticles, it appears that photocatalytic reactions could be quantitatively monitored as long as the concentration of R6G ranged from 10^{-6} M to 10^{-4} M. Over this concentration range, preliminary data suggest that there is a predictable, direct linear relationship between concentration of R6G and the integrated areas under curves fit to R6G peaks relative to that of the CS₂.

The generation of a preliminary calibration curve with the stabilized nanoparticles places the project in position to attempt to monitor photocatalytic reactions once again. With a more reliable calibration curve generation procedure now in place, quantitative information with regard to analyte concentration can be obtained from changes in spectral features in order to assess reaction kinetics. Also, the ability to maintain consistent signal even under a constant stir/pump setup allows monitoring reactions over a reasonable time period, and ensures that decreases in signal can be related to changes to molecular structure, and not simply a loss of signal due to nanoparticle destabilization. In practical application, it seems feasible that 1-decanethiol secondarily capped gold nanoparticle clusters can be used to monitor photocatalytic reactions over a period of 3-4 hours. This should be a sufficient amount of time, since the typical half-life for photocatalytic degradation of organic pollutants is under one hour.⁷³

CHAPTER 4

Summary/Future Directions: Effective Reaction Monitoring

Photocatalytic degradation is an important type of reaction in the context of wastewater treatment. It is attractive because it is highly efficient at breaking down harmful chemicals into harmless end products. It is established that this process uses energy from light to excite electrons in a photocatalyst such as TiO_2 , which generates reactive species in water that can break apart the harmful pollutants. However, the specific steps taken in the process of breaking down pollutants are not well understood, and it is not possible to ensure that using photocatalytic degradation in the wastewater treatment process is safe.

One tool that can be used to further study these reactions is Raman spectroscopy. Raman spectroscopy has several advantages over traditional methods, but the most important advantage is the rate of measurements. Spectra can already be collected once every 11 seconds over a 3-4 hour period, and consultation with computational data allows for determination of structural changes that are associated with changes in spectral features. Once it has been optimized, future work will employ a nanosecond pulsed laser to collect spectral data even faster, potentially several times per second. Since Raman spectroscopy can acquire information about the structure of molecules in solution much faster than traditional methods, it is more likely to identify intermediate reaction products which are too short-lived to detect with traditional methods. Thus, Raman spectroscopy is a useful complementary tool for identifying the intermediate products associated with a reaction,

consequently increasing the available information needed to piece together an accurate reaction mechanism. The discussed work sought to expand the applicability of Raman spectroscopy as an analytical tool for *in-situ* monitoring of photocatalytic degradation.

Despite the advantages offered by Raman studies, they are limited by a variety of factors which were addressed here. Raman spectroscopy has low sensitivity, which makes monitoring reactions of compounds which are lowly soluble or at concentrations realistic to wastewater treatment impossible without modification. The use of SERS greatly enhanced the sensitivity of Raman studies, allowing for the detection of some subsets of analytes at low concentrations. Additionally, SERS is not generally effective for quantitative analysis, which is important for assessing reaction rate. This was addressed by the introduction of an internal standard as a point of reference for accurate determination of changes in the concentration of a species as a function of time.

Initial attempts to monitor reactions led to the realization that nanoparticle stability is a concern for monitoring reactions using SERS. Since SERS is generally used as a detection method rather than a tool for monitoring changes over time; stability is not generally considered. However, if a reaction is to be monitored over an extended period of time, semi-aggregated nanoparticle clusters must maintain stability such that changes in signal are only due to changes in the composition of analytes in the solution, and not simply a result of excessive aggregation of nanoparticles causing signal diminishment. Nanoparticle stability was increased by the introduction of dilute amounts of 1-decanethiol, which sterically stabilized semi-aggregated nanoparticle clusters to prevent excessive aggregation. Maintenance of constant levels of signal over an extended time period via nanoparticle stabilization allows for reaction monitoring to occur.

The results of the experiments described in this thesis have provided the framework for monitoring photocatalytic reactions *in situ* via Raman spectroscopy with selected modifications that allow a wider variety of compounds to be analyzed. With these modifications established, the photocatalytic degradation of R6G, paraquat, and other cationic organic compounds can now be studied. Future reaction monitoring will include a series of three control trials prior to the experimental trial. The first compound which will be studied is R6G. In the first trial, a suspension of 1-decanethiol-secondarily-capped nanoparticle clusters which is 2% V/V CS₂ and 10⁻⁴ M R6G will be monitored for a period of 4 hr via the flowing setup depicted in Figure 2.8 in the absence of TiO₂ and UV radiation. A second control trial will contain the same constituents as trial one, but with the addition of a saturating amount of TiO₂, still in the absence of UV radiation. The third control trial will have the same constituents as trial one, but with the addition of constant exposure to UV radiation from the UV lamp, in the absence of TiO₂. The experimental trial contains all substituents of trial one, in the presence of both UV radiation and a saturating amount of TiO₂.

Most of the work discussed so far has been in reference to preliminary data which illustrate general principles with a model compound, R6G. Although these are crucial steps, R6G is not a particularly relevant compound in the context of wastewater treatment. It is important to be able to demonstrate that these processes will, once developed, be readily expanded into the study of more impactful degradation processes than that of R6G. It is easy to see how the ionic pesticide paraquat could be analyzed by essentially the same procedure as R6G, since it is also an organic cation, an important property which makes R6G so susceptible to this type of study. Steps for studying the degradation of paraquat

will be nearly identical to those for R6G, and since paraquat is such a commonly used pesticide, this will have more direct environmental impact. In fact, this procedure can serve as model for studying degradative reactions on any organic Raman active electrolyte.

The study of non-electrolyte species is more complicated, since they are not readily susceptible to SERS. This is largely due to a lack of a charged group which serves to bring the molecule into close proximity with the nanoparticle core. It may be possible in some cases to induce a charge on a particular compound by altering the pH of the solution. An alkaline solution can induce a negative charge, whereas an acidic solution can induce a positive charge. These induced charges caused by alterations in pH might allow for compounds which are not generally susceptible to SERS to be monitored. Additionally, this could serve to increase the aqueous solubility of some sparingly soluble compounds, since it would introduce polarity to an otherwise hydrophobic molecule. So, the applicability of SERS for use in monitoring photocatalytic reactions may be further expanded in future work by changing pH to induce charges on uncharged molecules to make them more susceptible to SERS.

The alteration of pH in order to visualize spectra of compounds which are not generally SERS active was not possible prior to nanoparticle stabilization. Citrate-capped gold nanoparticles alone are sensitive to changes in pH, and quickly aggregate. However, results from the recent studies of the 1-decanethiol capped semi-aggregated gold nanoparticles suggest that these nanoparticles would be more resistant to pH changes, and thus allow this hypothesis to be tested. Although it should be considered that studying reactions of a compound at greatly elevated or reduced pH will likely impact the overall

reaction mechanism, this is still an interesting possibility since it could potentially allow expansion of SERS reaction monitoring to a much broader category of compounds.

With some additional modifications to the SERS process, this approach could be applied to a wide variety of organic compounds, and may be extended to monitoring reactions other than photocatalytic degradation by simply altering the conditions of the reaction vessel, as long as the compounds of interest are susceptible to SERS. This project allows for *in situ* monitoring of reactions via Raman spectroscopy to be extended to a wider variety of compounds and their associated reactions, which will be the focus of future studies.

REFERENCES

1. Priscoli, J. D. Water and civilization: using history to reframe water policy debates and to build a new ecological realism. *Water Policy* **1**, 623–636 (2000).
2. E.B. Muller, A.H. Stouthamer, H.W. van Verseveld & D.H. Eikelboom. Aerobic domestic waste water treatment in a pilot plant with complete sludge retention by cross-flow filtration. *Water Res.* **29**, 1179–1189 (1995).
3. G. Bringmann & R. Kühn. Comparison of the toxicity thresholds of water pollutants to bacteria, algae, and protozoa in the cell multiplication inhibition test. *Water Res.* **13**, 231–241 (1980).
4. Hua, M., Zhang, S., Pan, B., Zhang, W., Lv, L. & Zhang, Q. Heavy metal removal from water/wastewater by nanosized metal oxides: A review. *J. Hazard. Mater.* **211-212**, 317–331 (2012).
5. Mallick, N. Biotechnological potential of immobilized algae for wastewater N, P and metal removal: a review. *Biometals* **15**, 377–390 (2002).
6. Wan Ngah, W. S. & Hanafiah, M. Removal of heavy metal ions from wastewater by chemically modified plant wastes as adsorbents: A review. *Bioresour. Technol.* **99**, 3935–3948 (2008).
7. Morales, H. A., Vidal, G., Olszewski, J., Rock, C., Dasgupta, D., Oshima, K. H. & Smith, G. B. Optimization of a Reusable Hollow-Fiber Ultrafilter for Simultaneous Concentration of Enteric Bacteria, Protozoa, and Viruses from Water. *Appl. Environ.*

- Microbiol.* **69**, 4098–4102 (2003).
8. Payment, P., Trudel, M. & Plante, R. Elimination of viruses and indicator bacteria at each step of treatment during preparation of drinking water at seven water treatment plants. *Appl. Environ. Microbiol.* **49**, 1418–1428 (1985).
 9. Hung, Y.-T., Aziz, H. A., Hassan, S. H., Yeh, R. L.-T., Liu, L.-H. & Butler, E. Chemical Waste and Allied Products. *Water Environ. Res.* **86**, 1447–1497 (2014).
 10. Bolto, B., Dixon, D., Eldridge, R., King, S. & Linge, K. Removal of natural organic matter by ion exchange. *Water Res.* **36**, 5057–5065 (2002).
 11. Dua, M., Singh, A., Sethunathan, N. & Johri, A. Biotechnology and bioremediation: successes and limitations. *Appl. Microbiol. Biotechnol.* **59**, 143–152 (2002).
 12. Stevens, A. A., Slocum, C. J., Seeger, D. R. & Robeck, G. G. Chlorination of organics in drinking water. *J. Am. Water Works Assoc.* 615–620 (1976).
 13. Von Gunten, U. Ozonation of drinking water: Part I. Oxidation kinetics and product formation. *Water Res.* **37**, 1443–1467 (2003).
 14. Das, R. Application Photocatalysis for Treatment of Industrial Waste Water—A Short Review. *OALib* **01**, 1–17 (2014).
 15. Blake, Daniel M. (2001). *Bibliography of Work on the Photocatalytic Removal of Hazardous Compounds from Water and Air*. Tech. Rep. NREL/TP-510-31319. Golden, CO: National Renewable Energy Laboratory. 265 pp. Available from the National Technical Information Service, Springfield, VA 22161.
 16. Konstantinou, I. K. & Albanis, T. A. TiO₂ -assisted photocatalytic degradation of azo dyes in aqueous solution: kinetic and mechanistic investigations. *Appl. Catal. B Environ.* **49**, 1–14 (2004).

17. Annarapu, S. & Nee, M. J. Thermal analysis of binding of iodinated contrast agents to TiO₂. *J. Therm. Anal. Calorim.* **116**, 1521–1526 (2014).
18. Ohko, Y., Iuchi, K.-I., Chisa, N., Tetsu, T., Tetsuto, N., Taisen, I., Yoshinoba, K. & Akira, F. 17 Beta-Estradiol Degradation by TiO₂ Photocatalysis as a Means of Reducing Estrogenic Activity. *Environ. Sci. Technol.* **36**, 4175–4181 (2002).
19. Salkic, S., Eckler, L. & Nee, M. Non-invasive monitoring of photocatalytic degradation of x-ray contrast media using Raman spectroscopy. *J. Raman Spectrosc.* **44**, 1746–1752 (2013).
20. Jeong, J., Jung, J., Cooper, W. J. & Song, W. Degradation mechanisms and kinetic studies for the treatment of X-ray contrast media compounds by advanced oxidation/reduction processes. *Water Res.* **44**, 4391–4398 (2010).
21. Lachheb, H., Puzenat, E., Houas, A., Ksibi, M., Elaloui, E., Guillard, C. & Herrmann, J.-M. Photocatalytic degradation of various types of dyes (Alizarin S, Crocein Orange G, Methyl Red, Congo Red, Methylene Blue) in water by UV-irradiated titania. *Appl. Catal. B Environ.* **39**, 75–90 (2002).
22. Buseti, F., Linge, K. L., Blythe, J. W. & Heitz, A. Rapid analysis of iodinated X-ray contrast media in secondary and tertiary treated wastewater by direct injection liquid chromatography-tandem mass spectrometry. *J. Chromatogr. A* **1213**, 200–208 (2008).
23. Dorsey, J. G. & Dill, K. A. The molecular mechanism of retention in reversed-phase liquid chromatography. *Chem. Rev.* **89**, 331–346 (1989).
24. Fenn, J. B., Mann, M., Meng, C. K., Wong, S. F. & Whitehouse, C. M. Electrospray ionization for mass spectrometry of large biomolecules. *Science* **246**, 64–71 (1989).

25. Houas, A., Lachheb, H., Ksibi, M., Elimame, E., Guillard, C. & Herrmann, J.-M. Photocatalytic degradation pathway of methylene blue in water. *Appl. Catal. B Environ.* **31**, 145–157 (2001).
26. Libowitzky, E. & Rossman, G. R. An IR absorption calibration for water in minerals. *Am. Mineral.* **82**, 1111–1115 (1997).
27. Sterling, T. M. Mechanisms of herbicide absorption across plant membranes and accumulation in plant cells. *Weed Sci.* 263–276 (1994).
28. Picó, Y., Font, G., Moltó, J. C. & Mañes, J. Solid-phase extraction of quaternary ammonium herbicides. *J. Chromatogr. A* **885**, 251–271 (2000).
29. Ensminger, M. P. & Hess, F. D. Photosynthesis involvement in the mechanism of action of diphenyl ether herbicides. *Plant Physiol.* **78**, 46–50 (1985).
30. Bus, J. S. & Gibson, J. E. Paraquat: model for oxidant-initiated toxicity. *Environ. Health Perspect.* **55**, 37 (1984).
31. Tanner, C. M., Kamel, F., Ross, G. W., Hoppin, J. A., Goldman, S. M., Korell, M., Marras, C., Bhudihikanok, G. S., Kasten, M., Chade, A. R., Comyns, K., Richards, M. B., Meng, C., Priestley, B., Fernandez, H. H., Cambi, F., Umbach, D. M., Blair, A., Sandler, D. P. & Langston, J. W. Rotenone, Paraquat, and Parkinson's Disease. *Environ. Health Perspect.* **119**, 866–872 (2011).
32. Bus, J. S., Aust, S. D. & Gibson, J. E. Paraquat toxicity: proposed mechanism of action involving lipid peroxidation. *Environ. Health Perspect.* **16**, 139 (1976).
33. Raman, C. V. A New Radiation. *Indian J. Phys.* **2**, 387 (1928).
34. Krishnan, K. A new class of spectra due to secondary radiation Part I. *Indian J. Phys.* **2**, 399–419 (1928).

35. Waterland, M. R., Stockwell, D. & Kelley, A. M. Symmetry breaking effects in NO_3^- : Raman spectra of nitrate salts and *ab initio* resonance Raman spectra of nitrate–water complexes. *J. Chem. Phys.* **114**, 6249 (2001).
36. Jamróz, M. H. Vibrational Energy Distribution Analysis (VEDA): Scopes and limitations. *Spectrochim. Acta. A Mol. Biomol. Spectrosc.* **114**, 220–230 (2013).
37. Stiles, P. L., Dieringer, J. A., Shah, N. C. & Van Duyne, R. P. Surface-Enhanced Raman Spectroscopy. *Annu. Rev. Anal. Chem.* **1**, 601–626 (2008).
38. McNay, G., Eustace, D., Smith, W. E., Faulds, K. & Graham, D. Surface-Enhanced Raman Scattering (SERS) and Surface-Enhanced Resonance Raman Scattering (SERRS): A Review of Applications. *Appl. Spectrosc.* **65**, 825–837 (2011).
39. Ansar, S. M., Li, X., Zou, S. & Zhang, D. Quantitative Comparison of Raman Activities, SERS Activities, and SERS Enhancement Factors of Organothiols: Implication to Chemical Enhancement. *J. Phys. Chem. Lett.* **3**, 560–565 (2012).
40. Moskovits, M. Surface-enhanced spectroscopy. *Rev. Mod. Phys.* **57**, 783 (1985).
41. Talley, C. E., Jackson, J. B., Oubre, C., Grady, N. K., Hollars, C. W., Lane, S. M., Huser, T. R., Nordlander, P. & Halas, N. J. Surface-Enhanced Raman Scattering from Individual Au Nanoparticles and Nanoparticle Dimer Substrates. *Nano Lett.* **5**, 1569–1574 (2005).
42. Champion, A. & Kambhampati, P. Surface-enhanced Raman scattering. *Chem. Soc. Rev.* **27**, 241–250 (1998).
43. Otto, A. The ‘chemical’ (electronic) contribution to surface-enhanced Raman scattering. *J. Raman Spectrosc.* **36**, 497–509 (2005).

44. Blackie, E. J., Ru, E. C. L. & Etchegoin, P. G. Single-Molecule Surface-Enhanced Raman Spectroscopy of Nonresonant Molecules. *J. Am. Chem. Soc.* **131**, 14466–14472 (2009).
45. Premasiri, W. R., Moir, D. T., Klempner, M. S., Krieger, N., Jones, G. & Ziegler, L. D. Characterization of the Surface Enhanced Raman Scattering (SERS) of Bacteria. *J. Phys. Chem. B* **109**, 312–320 (2005).
46. MacLaughlin, C. M., Mullaithilaga, N., Yang, G., Ip, S. Y., Wang, C. & Walker, G. C.. Surface-Enhanced Raman Scattering Dye-Labeled Au Nanoparticles for Triplexed Detection of Leukemia and Lymphoma Cells and SERS Flow Cytometry. *Langmuir* **29**, 1908–1919 (2013).
47. Han, X. X., Pienpinijtham, P., Zhao, B. & Ozaki, Y. Coupling Reaction-Based Ultrasensitive Detection of Phenolic Estrogens Using Surface-Enhanced Resonance Raman Scattering. *Anal. Chem.* **83**, 8582–8588 (2011).
48. Halvorson, R. A. & Vikesland, P. J. Surface-Enhanced Raman Spectroscopy (SERS) for Environmental Analyses. *Environ. Sci. Technol.* **44**, 7749–7755 (2010).
49. Lee, P. C. & Meisel, D. Adsorption and surface-enhanced Raman of dyes on silver and gold sols. *J. Phys. Chem.* **86**, 3391–3395 (1982).
50. Hong, S. & Li, X. Optimal Size of Gold Nanoparticles for Surface-Enhanced Raman Spectroscopy under Different Conditions. *J. Nanomater.* **2013**, 1–9 (2013).
51. Shaw, C. P. Fan, M., Lane, C., Barry, G., Jirasek, A. I. & Brolo, A. G. Statistical Correlation Between SERS Intensity and Nanoparticle Cluster Size. *J. Phys. Chem. C* **117**, 16596–16605 (2013).

52. Alberts, B., Johnson, A., Lewis, J., Morgan, D., Raff, M., Roberts, K., Walter, P. 2015. *Molecular Biology of the Cell*. Sixth Edition. New York (NY): Garland Science p.554–562.
53. Weitz, D. A. & Lin, M. Y. Dynamic scaling of cluster-mass distributions in kinetic colloid aggregation. *Phys. Rev. Lett.* **57**, 2037 (1986).
54. Talley, C. E., Jackson, J. B., Oubre, C., Grady, N. K., Hollars, C. W., Lane, S. M., Huser, T. R., Nordlander, P. & Halas, N. J. Surface-Enhanced Raman Scattering from Individual Au Nanoparticles and Nanoparticle Dimer Substrates. *Nano Lett.* **5**, 1569–1574 (2005).
55. Banholzer, M. J., Millstone, J. E., Qin, L. & Mirkin, C. A. Rationally designed nanostructures for surface-enhanced Raman spectroscopy. *Chem. Soc. Rev.* **37**, 885 (2008).
56. Wustholz, K. L., Henry, A.-I., McMahon, J. M., Freeman, R. Griffith., Valley, N., Piotti, M. E., Natan, M. J., Schatz, G. C. & Van Duyne, P. V. Structure–Activity Relationships in Gold Nanoparticle Dimers and Trimers for Surface-Enhanced Raman Spectroscopy. *J. Am. Chem. Soc.* **132**, 10903–10910 (2010).
57. Hoff, A. Correlation of Surface Enhanced Raman Spectroscopy and Nanoparticle Aggregation with Rhodamine 6G (2013). *Master's Theses: San Jose State University*. Paper 4390.
58. Skoog, D., West, D., Holler, F. J., Crouch, S. 2014. *Fundamentals of Analytical Chemistry*. Ninth Edition. Belmont (CA): Brooks/Cole.

59. Manson, J., Kumar, D., Meenan, B. J. & Dixon, D. Polyethylene glycol functionalized gold nanoparticles: the influence of capping density on stability in various media. *Gold Bull.* **44**, 99–105 (2011).
60. Kyrychenko, A., Karpushina, G. V., Svechkarev, D., Kolodezny, D., Bogatryenko, S. I., Kryshstal, A. P. & Doroshenko, A. O. Fluorescence Probing of Thiol-Functionalized Gold Nanoparticles: Is Alkylthiol Coating of a Nanoparticle as Hydrophobic as Expected? *J. Phys. Chem. C* **116**, 21059–21068 (2012).
61. Donaldson, P. M. & Hamm, P. Gold Nanoparticle Capping Layers: Structure, Dynamics, and Surface Enhancement Measured Using 2D-IR Spectroscopy. *Angew. Chem. Int. Ed.* **52**, 634–638 (2013).
62. Negishi, Y. Takasugi, Y., Sato, S., Yao, H., Kimura, K. & Tsukuda, T. Kinetic Stabilization of Growing Gold Clusters by Passivation with Thiolates. *J. Phys. Chem. B* **110**, 12218–12221 (2006).
63. Lin, S.-Y., Tsai, Y.-T., Chen, C.-C., Lin, C.-M. & Chen, C. Two-Step Functionalization of Neutral and Positively Charged Thiols onto Citrate-Stabilized Au Nanoparticles. *J. Phys. Chem. B* **108**, 2134–2139 (2004).
64. Kim, M.-K., Jeon, Y.-M., Jeon, W. S., Kim, H.-J., Hong, S. G., Park, C. G. & Kim, K. Novel dendron-stabilized gold nanoparticles with high stability and narrow size distribution. *Chem. Commun.* 667-668 (2001).
65. Kennedy, B. J., Milofsky, R. & Carron, K. T. Development of a cascade flow cell for dynamic aqueous phase detection using modified SERS substrates. *Anal. Chem.* **69**, 4708–4715 (1997).

66. Timothy Deschaines & Keith Carron. Stability and Surface Uniformity of Selected Thiol-Coated SERS Surfaces. *Appl. Spectrosc.* **51**, 1355–1359 (1997).
67. Lorén, A. Engelbrektsson, J., Ellasson, C., Josefson, M., Abrahamsson, J., Johansson, M. & Abrahamsson, K. Internal Standard in Surface-Enhanced Raman Spectroscopy. *Anal. Chem.* **76**, 7391–7395 (2004).
68. Bell, S. E. J. & Sirimuthu, N. M. S. Quantitative surface-enhanced Raman spectroscopy. *Chem. Soc. Rev.* **37**, 1012 (2008).
69. Ameer, F. S., Hu, W., Ansar, S. M., Siriwardana, K., Collier, W. E., Zou, S. & Zhang, D. Robust and Reproducible Quantification of SERS Enhancement Factors Using a Combination of Time-Resolved Raman Spectroscopy and Solvent Internal Reference Method. *J. Phys. Chem. C* **117**, 3483–3488 (2013).
70. Picard, A., Daniel, I., Montagnac, G. & Oger, P. In situ monitoring by quantitative Raman spectroscopy of alcoholic fermentation by *Saccharomyces cerevisiae* under high pressure. *Extremophiles* **11**, 445–452 (2007).
71. Aarnoutse, P. J. & Westerhuis, J. A. Quantitative Raman Reaction Monitoring Using the Solvent as Internal Standard. *Anal. Chem.* **77**, 1228–1236 (2005).
72. Moreno, T., Lopez, M. A. M., Illera, I. H., Piqueras, C. M., Arranz, A. S., Serna, J. G. & Cocero, M. J. Quantitative Raman determination of hydrogen peroxide using the solvent as internal standard: Online application in the direct synthesis of hydrogen peroxide. *Chem. Eng. J.* **166**, 1061–1065 (2011).
73. E. Pelizzetti, V. Maurino, C. Minero, O. Zerbini & E. Borgarello. Photocatalytic degradation of bentazon by TiO₂ particles. *Chemosphere* **18**, 1437–1445 (1989).